

General Disclaimer

One or more of the Following Statements may affect this Document

- This document has been reproduced from the best copy furnished by the organizational source. It is being released in the interest of making available as much information as possible.
- This document may contain data, which exceeds the sheet parameters. It was furnished in this condition by the organizational source and is the best copy available.
- This document may contain tone-on-tone or color graphs, charts and/or pictures, which have been reproduced in black and white.
- This document is paginated as submitted by the original source.
- Portions of this document are not fully legible due to the historical nature of some of the material. However, it is the best reproduction available from the original submission.

(NASA-CR-144329) OBSERVATIONS OF LIME
FLARES WITH A SOFT X-RAY TELESCOPE
(Aerospace Corp., El Segundo, Calif.) 69 p
HC \$4.50 CSCI 03B

Unclas
15228

16 February 1976

Prepared for
NATIONAL AERONAUTICS AND SPACE ADMINISTRATION
George C. Marshall Space Flight Center
Marshall Space Flight Center, Alabama 35812



Contract No. NAS8-29602



Laboratory Operations

THE AEROSPACE CORPORATION

OBSERVATIONS OF LIMB FLARES
WITH A SOFT X-RAY TELESCOPE

Prepared by
Edward G. Gibson
Space Sciences Laboratory

16 February 1976

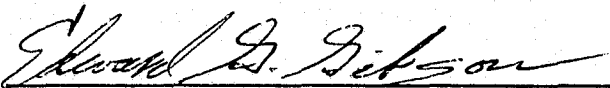
Laboratory Operations
THE AEROSPACE CORPORATION
El Segundo, Calif. 90245

Prepared for
NATIONAL AERONAUTICS AND SPACE ADMINISTRATION
George C. Marshall Space Flight Center
Marshall Space Flight Center, Alabama 35812

Contract No. NAS8-29602

OBSERVATIONS OF LIMB FLARES
WITH A SOFT X-RAY TELESCOPE

Prepared

A handwritten signature in cursive script, reading "Edward G. Gibson", written over a horizontal line.

Edward G. Gibson
Space Sciences Laboratory

Approved

A handwritten signature in cursive script, reading "George A. Paulikas", written over a horizontal line.

George A. Paulikas
Space Sciences Laboratory

ABSTRACT

The structure and evolution of 26 limb flares have been observed with a soft x-ray telescope flown on Skylab. The results are:

1. One or more well defined loops were the only structures of flare intensity observed during the rise phase and near flare maximum, except for knots which were close to the resolution of the telescope in size (≈ 2 arc seconds) and whose structure can therefore not be determined.
2. The flare core features were always sharply defined during the rise phase.
3. For the twenty events which contain loops, the geometry of the structure near maximum was that of a loop in ten cases, a loop with a spike at the top in four cases, a cusp or triangle in four cases, and a cusp combined with a spike in another two cases.
4. Of the fifteen cases in which sufficient data were available to allow us to follow a flare's evolution, five showed no significant geometrical deviation from a loop structure, one displayed little change except for a small scale short-lived perturbation on one side of the loop 10 seconds before a type III radio burst was observed, eight underwent a large scale deformation of the loop or loops on a time scale comparable to that of the flare itself and one double loop event changed in a complex and undetermined manner, with reconnection being one possibility.
5. The rise time, decay time and rate of increase of soft x-ray emission tended to increase with flare volume.
6. There were no correlations evident between either the maximum soft x-ray emission or the observation of non-thermal radio bursts with other flare observables.

PRECEDING PAGE BLANK NOT FILMED

7. The eight flares which underwent a large scale deformation tended to be thicker and have larger volumes, longer rise and decays times and smaller time rates of change of their soft x-ray emission in both the rise and decay phases.

Several flare theories are discussed relative to these observations.

Based on observation of the original film, it is suggested that the eight flares which underwent large scale deformations had become unstable to MHD kinks. This implies that these flares occurred in magnetic flux tubes through which significant currents were flowing.

It is also suggested the high energy electrons responsible for type III bursts accompanying these flares could have been accelerated by the $\vec{V} \times \vec{B}$ electric field induced by a small scale short-lived perturbation of part of a flaring flux tube, similar to the one perturbation which was observed having these characteristics.

CONTENTS

ABSTRACT	v
1. INTRODUCTION	1
2. STRUCTURE OF LIMB FLARES NEAR MAXIMUM	6
3. EVOLUTION OF LIMB FLARE STRUCTURE.....	11
4. CORRELATION OF LIMB FLARE STRUCTURES AND EVOLUTION WITH OTHER OBSERVABLES	17
5. SUMMARY	27
6. DISCUSSION	29
ACKNOWLEDGMENTS	39
FIGURES	40
REFERENCES	61

TABLES

1. Characteristics of X-Ray Filters	2
2. Frequency of Occurrence of Categories of Flare Cores Observed Near Flare Maximum	8
3. Summary of Flare Loop Evolutions	16
4. Correlation Coefficients Between Pairs of Observables	21
5. Categories of Correlation	22

FIGURES

1.	Limb Flare Loop	42
2.	Measurements Made on Limb Flare Loops	43
3.	Triangular Flare Loop Geometry Near Maximum	44
4.	Small Scale Flare Loop Perturbation Immediately Preceding a Type III Radio Burst	45
5.	Large Scale Deformation of a Flare Loop	46
6.	Measured 2-8Å Soft X-ray Flux for the Flare shown in Figure 5	47
7.	A Two Loop Flare	48
8.	Measured 2-8Å Soft X-ray Flux for the Flare shown in Figure 7	49
9.	Flare Loop Geometry Correlations	50
10.	Rise Time, Decay Time and Flare Volume Correlations	52
11.	SOLRAD Peak Flare Intensity Correlation with Flare Volume	55
12.	Correlations of the Characteristic Rates of Rise and Decay of Soft X-Ray Emission with Flare Volume	56
13.	Correlations of Evidence for Kink Evolution with Other Flare Observables	58
14.	Sample Correlation Coefficients and 95% Limits of Confidence for All Correlations Studied	60

1. INTRODUCTION

The soft x-ray data from the S-056 Skylab/ATM instrument were examined with the anticipation that the observed morphology could yield significant information about the mechanism of magnetic energy storage, the type of instability which initiates the flare process and the mode of energy release. The results of an initial study of 132 disc and limb flare cores observed during the three Skylab missions by the S-056 experiment have recently been reported (Vorpahl, et al., 1976) and are hereafter referred to as the Initial Study. Because of the interesting nature of these results and the greater visibility of flare geometry obtained by viewing a flare from the side, a more detailed study of limb flares ($R/R_{\odot} \geq 0.90$) was undertaken. The manner in which the flare data were obtained and the results of the Initial Study are briefly reviewed before the present study of 26 limb events is discussed.

The S-056 Soft X-ray Telescope was part of the cluster of ATM instruments flown on Skylab from May 1973 to February 1974. A detailed description of the experiment is given elsewhere (Underwood et al., 1976) but is very briefly summarized here. The telescope used polished fused silica optics arranged in a Wolter type I configuration with an effective focal length of 190.3 cm and a collecting area of 14.8 cm^2 . Any one of five thin metal filters could be inserted into the optical path immediately in front of the focal plane and provide some spectral discrimination (Table 1). In addition to the telescope, the S-056 experiment also contained an X-Ray Event Analyzer (X-REA) which monitored the total soft x-ray flux from the sun in two wavelength ranges with a time resolution of 2.5 seconds. It consisted of two uncollimated proportional counters that had an aluminum window ($8\text{-}20\text{\AA}$, 1.71 mg/cm^2) and

TABLE 1

CHARACTERISTICS OF X-RAY FILTERS

Filter No.	Material	Thickness (mg/cm ²)	Bandpass* (A)
1	aluminum	3.45	8-16
2	aluminum	1.56	8-22
3	titanium	0.99	6-14 and 27-47
4	beryllium	4.60	6-18
5	beryllium	13.1	6-13

*Wavelength region where the product of filter transmission and telescope reflectivity exceed 10^{-4} .

a beryllium window ($2\text{-}8\text{\AA}$, 46.9 mg/cm^2) respectively. Pulse height analysis was performed onboard to obtain spectral information.

The S-056 telescope and X-REA proved to be excellent instruments for obtaining good quality data on many flares. The spatial resolution at the center of the telescope's field of view was approximately 2 arc seconds which permitted good definition of flare features. A large number of flares were observed for two reasons. First, the telescope's wide field of view (40 arc minutes) meant that many flares were observed even when the instrument was not pointed directly at the flaring active region. Second, an abundant supply of film was always available so that the instrument was operated during nearly every observing sequence. Over 27,000 frames of solar data were obtained from the three missions. Thus, even though the ATM was observing other phenomena, data were often obtained on any one or all phases of a flare; preflare, rise, peak and decay. The abundant supply of film also permitted the operator to start the instrument in the mode of rapid data acquisition at the slightest indication of a transient event. This mode cycled through filters 1, 3 and 5 with 1.25 second exposures and 9 seconds between exposures. Because of these two factors, several hundred transient flare-like brightenings were observed. Good supporting data from the X-REA were almost always available since it continuously observed the total solar soft x-ray flux when a crew member was operating the ATM.

The Initial Study revealed that the core of soft x-ray emission from a flare near maximum was composed of one or more sharply defined features and was surrounded by fainter and more diffuse emission. The most

characteristic feature of a flare core was a linear feature that was often arch shaped and resembled a loop, especially when viewed close to the limb. Two or more loops were often present, sometimes closely spaced and other times in the form of a longer arcade. These linear features were continuously distributed in length with a maximum frequency of occurrence in the range of 5 to 25 arc seconds. When a flare core feature was less than 10 arc seconds in size, it became more difficult to determine from the data whether it was linear or resembled a loop. Therefore, when a core feature was less than 10 arc seconds in size and its length-to-width ratio was less than two, it was designated as a knot. In the Initial Study it was suggested that knots defined in this way were unresolvable loops.

In approximately 80% of the flares that were observed with sufficient coverage in time, the loops did not significantly change shape as the flare evolved, even though new loops or knots would sometimes appear and cause a second rise in the total soft x-ray emission. There was no significant correlation observed between the flare size and either of the following:

- 1) the flare rise time, defined by the time between the 10% and 90% of maximum points in the history of the total counts from the 2-8Å beryllium proportional counter, or
- 2) the presence of high energy non-thermal electrons, indicated by either impulsive radio bursts at or above 2000 MHz or type III bursts.

In general, it was concluded that loops were fundamental structures in the flare cores. In most cases the soft x-ray emission was distributed continuously along a loop as it flared, although it was usually more intense at the top than the footpoints. In only about 25% of the flares were there knots of soft x-ray

emission which were close to the limit of resolution of the telescope in size. When a knot existed with a loop, it was usually near one of the footpoints of the loop rather than at the top. Thus, the Initial Study did not show evidence for a highly concentrated energy release, at a magnetic neutral point, for example, but did imply that loops are a fundamental structure in the flare process. This result must be qualified, however, by noting that the soft x-rays could have been emitted from a larger and relatively cooler plasma volume compared with the source of the relatively concentrated emission observed in highly ionized iron XUV lines (Cheng and Widing, 1975). Also, the possibility cannot be excluded at present that the initial energy release took place in a time (a few seconds) which was short compared with the time between the soft x-ray exposures.

2. STRUCTURE OF LIMB FLARES NEAR MAXIMUM

A fruitful first step in studying the morphology of limb flares observed in soft x-rays is to analyze their structure near flare maximum. The Initial Study showed that most of the core features did not change shape significantly during a flare. Thus, the core features observed near maximum can usually be considered as a characteristic property of the flare lasting most of its life.

In order to obtain a measure of the total soft x-ray emission from a flare, the peak intensity from the $1-8\text{\AA}$ channel of Solrad 9 or Solrad 10 reported in Solar Geophysical Data has been used. When SOLRAD records were not available, the total count from the X-REA $2-8\text{\AA}$ Be counter was used to determine an equivalent SOLRAD intensity. Since the sensitivity of the X-REA counters degraded with mission duration, a calibration curve giving the ratio of X-REA Be total counts ($2-8\text{\AA}$) to SOLRAD ($1-8\text{\AA}$) intensity versus time during the three Skylab missions was determined using 395 flare events for which this ratio was available. Twenty of the 26 limb flares under discussion here had intensities greater than or equal to a C1 flare ($10^{-3} \text{ ergs/cm}^2 \text{ - sec}$). The remaining six had intensities between 0.1 and 1.0 of a C1 flare.

Three criteria were used in selecting the flares to be studied. First, the X-REA Be total counts curve must have had a well-defined signature that was at least a factor of two above background. Second, the flare core must have been relatively very bright and easily identified on the film near flare maximum. Last, the central distance of the flare from disc center, R/R_{\odot} , must have been greater than 0.90. In those cases in which multiple

events in the X-REA Be total counts were observed, the peak of the second event was always at least a factor of ten greater than the level to which the first event had decayed.

The results are summarized in Table 2 where the system used to describe the features in a flare core is the same as presented in the Initial Study; e.g., L refers to a loop, K to a knot, 2L or 2K to two loops or knots respectively and KL + L to a knot on a loop plus a second loop. A major result of these observations is that whenever the core feature is large enough to be clearly resolved (≥ 10 arc seconds), it is in the shape of a loop or arch (Figure 1). This is true except in one case where the feature appeared to be viewed in the plane of the arch. Thus, the suggestion made in the Initial Study that the linear features seen on the disk are most likely loops, is supported here. From Table 2 it is seen that flare cores that contain knots constitute only 27% of all cores observed. This is very close to the corresponding value of 24% found in the Initial Study. Also, it is seen that the ratio of the number of single loops to single knots is approximately 3, which is also in agreement with the Initial Study. However, in the Initial Study, 42% of the 132 cores contained two or more loops, while here the corresponding number is only 16%. One possible reason for this is the difficulty of distinguishing overlapping loops at the limb, especially when one is significantly brighter than the other.

All loops have been measured visually using a positive copy of the film once removed from the original film, a light table and calibrated optics. The distance between footpoints (F), the height (H) and the mean thickness (T) were measured (Figure 2). A consideration relative to the ability to see the

TABLE 2

FREQUENCY OF OCCURRENCE OF CATEGORIES OF
FLARE CORES OBSERVED NEAR FLARE MAXIMUM

Category of Flare Core	Number Observed	Percent
Simple L	16	61
K	5	19
Complex 2L	3	12
2K	1	4
KL + L	1	4
	26	100

footpoints is that several of the loops were very close to the limb ($R/R_{\odot} \approx 1.0$) but only one was over the limb (10° in longitude or approximately 10,000 km occultation). This event will be discussed shortly.

Two physically significant variations of the loop structure near flare maximum were observed. The first one, which was mentioned in the Initial Study and was observed six times here, is the vertical spike or small streamer over the loop (Figure 3a)*. When present, it was very faint relative to the loop and leaves open the possibility that spikes may have existed in flares other than the six out of the 26 in which they were observed. They were usually seen in the flare rise and persisted through maximum, but were not seen during flare decay.

The second variation to the loop structure is that of a cusp or nearly triangular geometry (Figure 3b). This was also observed in six out of the 26 limb flares studied with only two of them being common to the set which also displayed spikes. The first flare which displayed both spike and cusp geometries is shown in Figure 3a. The second one will be discussed shortly. It could be argued that the cusp or triangle is not really a variation of a loop

* There is no substitute for viewing the first or second generation films directly. The much greater dynamic range of density on the film allows one to recognize patterns and features that, at present, cannot be reproduced in print. In this sense, the reader is dependent upon the interpretations of the films by the author, which is bound to raise controversy when substantial issues are involved. However, until greatly improved photographic reproduction capabilities are available, these interpretations must also be regarded as a form of data presentation, which can always be checked by interested parties who may also directly view the film.

at all, but rather is a separate and unique geometrical structure. To answer this and to explore some other significant observations, we now turn to the evolution of the limb events.

3. EVOLUTION OF LIMB FLARE STRUCTURE

In 15 out of the 20 limb events which contained recognizable loops, sufficient data were available to determine what changes, if any, occurred in the structure during the flare. These 15 events can be divided into three categories.

In the first category, which contains six of the events, no major geometrical change occurred. During the flare rise, the loop brightened and became more sharply defined. During the decay, it simply faded out and became more diffuse. In the Initial Study, approximately 80% of all flares were observed to behave in this manner. The difference can be accounted for by our increased ability to see more subtle structural changes that take place in the plane containing the flare loop, which is approximately perpendicular to the solar surface. This is made possible by our full or partial broadside view of the flare. One characteristic which was common to all flares investigated here and in the Initial Study, however, is the characteristic of being sharply defined in the rise phase.

A very significant observation of a small change on one of the flare loops, which otherwise remained static during flare evolution, is shown in Figure 4. At 1425:02 UT on 15 January 1974, it is seen that a small scale perturbation resembling a kink or spike on the left-hand side of the loop appeared. It was not evident 27 seconds later. The original film suggests more strongly that it was a kink than the reproduction shown here. Of significance is the fact that a type III burst was observed from 1425:12 to 1425:48 UT. It was an intensity 1 burst ($8 \text{ to } 80 \times 10^{22} \text{ watts/m}^2 \text{ Hz}$) observed by Sagamore

Hill Radio Observatory in the 24 - 48 MHz range. Thus, the perturbation to the loop occurred at least 10 seconds, but less than 38 seconds before a burst of non-thermal electrons moved outward through the inner corona. No other features of flare intensity were on the disk during this event. If electrons left the perturbation at a speed of $0.2c$, they would have traveled $0.86 R_{\odot}$ in ten seconds. This is a reasonable distance for the approximate height above an active region at which the electron density has decreased to $3 \times 10^7 \text{ cm}^{-3}$, the density corresponding to a plasma frequency of 48 MHz. Also, the acceleration required to produce the feature was large; the perturbation moved at least two arc seconds away from the loop axis in a time of less than 32 seconds, implying a velocity of 91 cm/sec and a mean acceleration of 2.8 km/sec^2 , approximately ten times solar gravity. This observation is unique among the 26 limb events studied. However, the difficulty of making the observation is considerable and the event should therefore not necessarily be considered rare. That is, the instrument must have been in the mode of rapid data acquisition early in the flare rise when type III bursts normally occur. Also, out of the 26 limb flares, only seven were observed to coincide with evidence of the bursts of non-thermal electrons; either a type III or non-thermal radio bursts.

The second major category of loop evolution is shown in Figure 5a. It is seen that the whole loop underwent a large scale deformation which evolved with the same time scale as the total x-ray flux from the flare, in contrast to the event just discussed in which only part of the loop participated and which lasted less than one minute. It is the opinion of the author that the deformation

observed in the original film is very suggestive of the kinking or buckling which is depicted in Figure 5b. However, no claim is made here for having proven the exact correspondence between Figures 5a and 5b^{*}. This type of large scale deformation was observed in 8 of 20 limb flares which contained loops. For convenience of discussion, the sequence of change is denoted by stages I to IV as shown in Figure 5b. Stage I is the undeformed loops. The center of the loop moves up and appears to kink as stage II is reached. Stage III implies that the motion of the sides of the loop may continue towards the loop center past one another and cross. Stage IV shows the flare core at slightly past flare maximum and having a triangular shape, a feature seen in other flares near maximum. The other variation of a loop structure near flare maximum, a spike, was barely visible on the first generation film in stage I with a slight amount of emission extending from its right side. This was not common to all "kink" flares and is not necessary for the definition of stage I. For subsequent analysis, a flare was considered to undergo a "kink" evolution if two or more of the four stages were observed.

The flare shown in Figure 5a is also the one event which had a knot intersecting a loop (KL). The knot is seen at the left footpoint in stage II. This is somewhat surprising since the center of the active region from which this flare is suspected to originate (Boulder 314), was 10° past the limb and the bottom 10,000 km was occulted. The flare was not observed in H α by ground

* Evidence for a kink instability in a solar flare in the XUV NRL ATM data has also recently been found (Cheng, 1975).

based observatories. On the previous day, a soft x-ray flare was observed with good time coverage from this region. In this event, the loop was not deformed but remained static as it faded. It is possible that the bottom 10,000 km was occulted, but it is more likely that the event occurred significantly further east (toward the limb) than the center of the active region in which it was assumed to originate.

Besides having a knot intersecting a loop, this flare is counted as one having two loops (LK + L). The evidence for the second one, although an appreciably fainter loop, is seen in Figure 5a, to the left of the main loop in stages II and III. It appears to assume approximately the same configuration as the main loop in stages II and III but is not as bright or sharply defined. Evidence for the second loop in stages I and IV does exist on the original film, but does not appear here because the reproductions have been optimized for the main loop.

The time history displayed in Figure 6 shows that the soft x-ray emission started to increase rapidly at 2138 UT and reached a plateau at 2144 UT. A further but slower increase in emission started at 2149 UT and reached a peak at 2200 UT corresponding to stage III. It is not possible to directly relate this two-stage rise to the successive appearance of the two loops. That is, if the initial rise was due to the second loop, this loop should have been brighter in the stage I observation at 2148 UT. On the other hand, if the second rise was due to the second loop, it should have been brighter in the stages II and III observations. Since the second loop is always fainter, it must be concluded that the main loop, and possibly both loops, experienced a two-stage rise in soft x-ray emission.

The third category of loop evolution observed contains only one example in this sample of limb flares. This event, shown in Figure 7, does show significant structural change but does not have any obvious characteristics of the "kink" evolution. At 1515:57 UT two loops were bright. By 1517:19 UT the geometry resembled that of a single loop. From Figure 8 it is seen that this time is very close to maximum in the soft x-ray emission at approximately 1517:30 UT. As the flare decays from 1517:46 UT to 1519:09 UT no recognizable feature can be discerned. The available data on this event, however, are not sufficient to state with precision what has really taken place. It may have been either a reconnection with two loops becoming one, or some other type of evolution for which we have no other examples.

Table 3 summarizes the evolutions observed in the 20 limb flares that contained loops.

TABLE 3

SUMMARY OF FLARE LOOP EVOLUTIONS

Type	Number Observed
Static	6
"Kink" Observation	8
Possible Reconnection	1
Insufficient data to determine	5
TOTAL	20

4. CORRELATION OF LIMB FLARE STRUCTURES AND EVOLUTION WITH OTHER OBSERVABLES

The variables that are available to correlate with one another originate from three sources.

First, the film data contains information on the type of flare core (L, K, KL, etc.), the size of a loop (F, H, T - see Figure 2) and the presence or absence of a large scale deformation which has been interpreted here as a kink instability. The volume (V) of a loop, like that shown in Figure 2, is calculated using the following approximate relation

$$V = (2H + F) (\pi T^2/4) \quad (1)$$

That is, the loop is approximated in total length by three sides of a rectangle, two sides of length H and one of length F, and in cross sectional area by a circle of diameter T. This tends to overestimate the length. However, since our line of sight is rarely perpendicular to the distance between footpoints, F is almost always an underestimate and the two estimates err in compensating directions. Our lack of precise knowledge of the geometry does not warrant a more exact formula. Since the knots are too small to have a clearly defined structure, a quantitative estimate of their volume is not included in the present study.

The measured values of T used in equation 1 fall in the range of three to seven arc seconds. Since the resolution of the telescope was approximately two arc seconds, it is difficult to make these measurements with precision. This coupled with the facts that the thickness was usually nonuniform along a loop and the cross section was most likely not perfectly circular is responsible

for much of the spread in the correlation data involving either T or especially V , which varies as T^2 .

The second source of data is the record of the X-REA Be total counts for each flare that gives three observables; the peak value of soft x-ray flux (I_p), the rise time (τ_R) and the decay times (τ_D). The peak flux, I_p , is computed in units of equivalent SOLRAD (1-8Å) flux units using the previously mentioned calibration curve in those cases where SOLRAD data is not available. The rise and decay times are e-folding times measured directly from the X-REA records (Figures 6 and 8). In most cases the decay with time is exponential over a sizeable period past flare maximum. On the other hand, the rise tends to be somewhat more complex but usually a sufficient period of approximately exponential change exists immediately preceding the flare maximum so that meaningful values of τ_R can be determined. Although the absolute values of τ_R and τ_D will, in general, be different for the radiative flux observed in different wavelength regions, the relative values of the τ_R 's and τ_D 's used here are meaningful when comparing the characteristics of one flare to another. A measure of the time rates of change of the soft x-ray emission during flare rise and flare decay can be also calculated simply by the ratios I_p/τ_R and I_p/τ_D , respectively.

Lastly, each flare is regarded to be positive or negative with respect to two observables. The first is the presence or absence of an observable quantity of energetic non-thermal electrons during the rise phase. Since hard x-ray data is not available on most of the flares studied, the presence of these electrons is taken to be indicated by non-thermal radio bursts

(NTRB); either a type III radio burst or an impulsive radio burst above 2000 MHz during the rise period. The second observable is the presence or absence of evidence for a "kink" type of evolution already discussed.

In total, there are eleven quantities that can be used in the study resulting in 55 possible correlations. However, correlations between variables in which one is dependent on the other are not made; e.g., F and V or τ_R and I_p/τ_R . Also, the correlation between F and other observables is not calculated, except for H , because of the large but unknown variation of our measurement of F introduced by the varying angle between our line of sight and the line between loop footpoints. In this way, the resulting number of independent correlations calculated is reduced to 39.

A measure of the correlation between observables is obtained in two ways. First, one observable is plotted against another and the correlation obtained by inspection (Figures 9 to 13). Although useful, this method is too subjective and correlation coefficients were therefore calculated. For any two observables, which occur in pairs, X_i and Y_i , a correlation coefficient r , can be defined by

$$r = \frac{\sum_i (X_i - \bar{X})(Y_i - \bar{Y})}{\left[\sum_i (X_i - \bar{X})^2 \sum_i (Y_i - \bar{Y})^2 \right]^{\frac{1}{2}}} \quad (2)$$

where \bar{X} and \bar{Y} are the arithmetic mean of all n values of X_i and Y_i , respectively, and the summations are made over all n (Beyer, 1966). Perfect positive

(negative) correlation corresponds to a value of +1.0 (-1.0) for r and no correlation corresponds to a value of 0. The results of these calculations are given in Table 4 and Figure 14. Equation (2) was also applied to the cases of the NTRB and "kink" observation data in which one variable can assume only two values; C_1 and C_2 . Values of +1 and -1 were used here although inspection of equation (1) shows that the result would be unaltered for any other two real values selected.

From a statistical standpoint, the number of pairs of samples available for correlation (13 to 26) is relatively small. Thus, it is useful to ask what value r would assume if the number of sample pairs was unlimited. Our knowledge of this value, termed the population correlation coefficient and denoted by ρ , has limits which can be calculated from statistical theory (Beyer, 1966). Given n and the value of r calculated using the n pairs of data, which are assumed to be sampled at random from the unlimited number in the population distribution, an upper and a lower limit on ρ is calculated with a corresponding level of confidence. These limits on ρ are shown in Table 4 and Figure 14 corresponding to a confidence of 95%. It should be noted that the actual value of ρ excludes the random errors made in acquiring the original data but not the systematic ones.

The observed correlation between pairs of observables can be divided into three categories as shown in Table 5.

Although the division between these categories is somewhat arbitrary, the general level of correlation which they define does have meaning. Negligible correlation means that the present study shows that the two observables

TABLE 4

CORRELATION COEFFICIENTS BETWEEN PAIRS OF OBSERVABLES

Observables		Number of Sample Pairs, n	Sample Correlation Coefficient, r	95% Confidence Limits for Population Correlation coefficient, ρ		Category of Correlation
Y	X			Lower limit	Upper limit	
F	H	20	+0.132	-0.32	+0.53	0
T	H	20	+0.304	-0.16	+0.65	0
log R	H	17	+0.232	-0.27	+0.63	0
	T	17	+0.315	-0.20	+0.68	0
	log V	16	+0.709	+0.32	+0.87	++
log τ_D	H	18	+0.334	-0.16	+0.68	0
	T	18	+0.564	+0.13	+0.81	+
	log V	17	+0.714	+0.35	+0.87	++
	log τ_R	21	+0.520	+0.11	+0.77	+
log I_p	H	20	-0.353	-0.68	+0.10	0
	T	20	-0.148	-0.54	+0.31	0
	log V	19	-0.317	-0.67	+0.16	0
	log τ_R	21	-0.093	-0.49	+0.35	0
	log τ_D	23	-0.292	-0.62	+0.14	0
log(I_p/τ_R)	H	17	-0.293	-0.68	+0.22	0
	T	17	-0.628	-0.84	-0.20	-
	log V	16	-0.762	-0.90	-0.44	--
	log τ_D	21	-0.642	-0.83	-0.29	-
log(I_p/τ_D)	H	18	-0.356	-0.70	+0.13	0
	T	18	-0.543	-0.79	-0.10	-
	log V	17	-0.434	-0.73	+0.07	0
	log τ_R	21	-0.167	-0.55	+0.28	0
Non-Thermal Radio Bursts	H	20	-0.321	-0.66	+0.14	0
	T	20	-0.243	-0.60	+0.22	0
	log V	19	-0.315	-0.67	+0.16	0
	log τ_R	21	-0.119	-0.51	+0.33	0
	log τ_D	22	-0.100	-0.49	+0.33	0
	log I_p	26	+0.148	-0.25	+0.53	0
	log(I_p/τ_R)	21	-0.083	-0.51	+0.36	0
"Kink" Observation	log(I_p/τ_D)	23	+0.189	-0.24	+0.55	0
	H	15	+0.258	-0.29	+0.67	0
	T	15	+0.633	+0.18	+0.85	+
	log V	15	+0.554	+0.06	+0.82	+
	log τ_R	13	+0.578	+0.04	+0.84	+
	log τ_D	14	+0.737	+0.32	+0.90	++
	log I_p	15	-0.456	-0.77	+0.07	0
	log(I_p/τ_R)	13	-0.847	-0.54	-0.94	--
	log(I_p/τ_D)	14	-0.598	-0.85	-0.10	-
	NTRB	15	-0.111	-0.57	+0.42	0

TABLE 5

CATEGORIES OF CORRELATION*

Category	r	95% confidence limits on ρ
Negligible: 0	$ r < 0.5$	includes $\rho = 0$
Weak: + or -	$0.5 \leq r < 0.7$	does not include $\rho = 0$
Significant: ++ or --	$0.7 \leq r \leq 1.0$	$ \text{both } \rho \text{ limits} > 0.3$

are essentially independent of one another. Weak correlation suggests that a dependence may exist while significant correlation means that a definite correlation does exist. Of the 39 correlations made, 25 are negligible, 9 are weak and only 5 are significant. The specific results are now described.

Unexpectedly, the dimensions of the flare loops show negligible correlation with one another ($r [F/H] = 0.13$ and $r[T/H] = 0.30$). A large amount of the scatter present in the plot of F with H (Figure 9a) is due to the unrestricted and unknown variation of the angle between our line of sight and the line between footpoints. It is probable that many of the values of F/H which fall in the range of 0.5 to 1.5 really lie in the range of 1.5 to 3 and that the real correlation is correspondingly higher. The data point with the arrow in Figure 9a, and subsequent figures is for a flare which appears to be viewed in the plane of the arch. The arrow indicates the direction that the data point would move, if we had viewed it broadside. In Figure 9b, it is seen that there is only a negligible tendency for the loops that extend higher in the atmosphere to also be thicker.

The log of the rise time, $\log \tau_R$, does not correlate with either H or T . This is consistent with the absence of correlation between rise time and flare size found in the Initial Study. However, $\log \tau_R$ does show a significant positive correlation with $\log V$ (Figure 10a, $r[\log \tau_R / \log V] = 0.71$). The values of the logarithms are used here and in many of the correlations because of the wide dynamic range of many of the variables. Essentially the same correlations hold true for $\log \tau_D$ (Figure 10b, $r[\log \tau_D / \log V] = 0.71$), except that the correlation with T is strong enough to be weakly positive. The correlation

between $\log \tau_R$ and $\log \tau_D$ is only weakly positive (Figure 10c). Thus, the fact that both correlation coefficients for $\log \tau_R$ and $\log \tau_D$ with $\log V$ are nearly 0.71 (0.709 and 0.714) must be fortuitous. In Figure 10c it is seen that the rise and decay times of the flares which have knots (K) are not distinguishable from those which do not.

The log of the peak intensity in the SOLRAD 1-8 Å channel or the X-REA equivalent, $\log I_p$, shows no correlation with any of the other observables. However, in Figure 11 a stronger negative correlation with $\log V$ is suggested than is calculated ($r[\log I_p / \log V] = -0.32$). Inspection shows that the negative correlation is fairly strong for flares of size C2 ($I_p = 2 \times 10^{-3}$ ergs/cm²sec) and smaller. Larger flares tend to have a wider spread in volume. Also noteworthy here, however, is that the six flares which contain only knots have peak fluxes between 10^{-3} and 10^{-2} ergs/cm²sec. Because of the small volume of these flares, this should tend to increase the correlation.

When the characteristic rate of rise of the soft x-ray emission is considered, I_p / τ_R , it is seen that the log of its value has a significant negative correlation with $\log V$ (Figure 12a, $r[\log(I_p / \tau_R) / \log V] = -0.76$). This is consistent with the previously mentioned manner in which $\log \tau_R$ and $\log I_p$ correlate with $\log V$. $\log(I_p / \tau_R)$ also has a weak negative correlation with T and $\log \tau_D$. In contrast, the rate of decay of soft x-ray emission does not correlate as well with other observables. The values of $\log(I_p / \tau_D)$ display only a weak negative correlation with T and a negligible correlation with $\log V$ (Figure 12b, $r[\log(I_p / \tau_D) / \log V] = -0.43$).

The presence or absence of any observable energetic non-thermal electrons during flare rise, determined by the presence of non-thermal radio bursts (NTRB), has negligible correlation with all other observables. In all cases, $|r| < 0.32$. This is consistent with the Initial Study which found no apparent correlation between the presence of NTRB's and the size of flare core features, loops or knots. Also, in the present study, none of the seven flare cores which contain one or more knots correspond to flares with NTRB's. The Initial Study indicated that approximately one out of every four flare cores which have NTRB's also have a feature of less than 10 arc seconds in size. The result obtained here can be attributed to the relatively small number of flare cores investigated (26 compared to 132 in the Initial Study).

The presence or absence of evidence of a "kink" type evolution (large scale deformation) shows the largest correlation with other observables (Figure 13). In fact, the largest correlation of this study is between the "kink" observation and $\log(I_p / \tau_R)$ (Figure 13f, $r = 0.85$). The "kink" observation also shows a significant positive correlation with $\log \tau_D$ (Figure 13d, $r = +0.74$). Weak positive correlations are found with T , $\log V$ and $\log \tau_R$ and a weak negative correlation is found with $\log I_p / \tau_D$. Thus, flare loops which show evidence of a "kink" type of evolution tend to be thicker, have a larger volume, rise and decay relatively slowly and have correspondingly lower time rates of change of soft x-ray emission. It should also be noted that there is negligible correlation with H , $\log I_p$ and the presence or absence of NTRB's.

One last correlation remains to be discussed. It is natural to anticipate that limb flares are good candidates for the creation of observable coronal transients. Thus, the observations of the corona made by the High Altitude Observatory Coronagraph, also flown on ATM, have been examined. It is found that none of the 26 flares that have been investigated here correspond to any recognizable coronal transients or major restructuring of coronal features. In some instances observations of the corona were available 10 to 20 minutes after flare rise but in others many hours had elapsed. Although this completely negative result is unexpected, a low correlation is consistent with what has recently been learned about coronal transients (Munro, et al., 1974):

1. More energetic flares have a high probability of producing observable transients. All of the flares studied here were smaller than M1 with one exception.
2. Eruptive prominences produce approximately three times the number of coronal transients as do flares. The flares observed here had no associated eruptive prominences.
3. Flares which eject material have a much higher correlation with observed coronal transients than do those which do not. There were no reported material ejections for any of the flares studied here.

5. SUMMARY

The observation of twenty six limb flares in soft x-rays yields the following results:

1. One or more well defined loops were the only structures observed of flare intensity during the flare rise phase and near flare maximum, except for knots which were close to the resolution of the telescope in size. The structure of these knots was too small to be determined. This is consistent with the Initial Study.
2. The flare core features were always sharply defined during the rise phase. This also is consistent with the Initial Study.
3. For the twenty events which contain loops, the geometry of the structure near maximum was that of a loop in ten cases, a loop with a spike on top in four cases, a cusp or triangle in four cases, and a cusp combined with a spike in another two cases.
4. Of the fifteen cases in which sufficient data were available to allow us to follow a flare's evolution, five showed no significant geometrical deviation from a loop structure, one displayed little change, except for a short-lived perturbation on one side of the loop immediately before a type III burst was observed, eight underwent a large scale deformation of the loop or loops on a time scale comparable to that of the flare itself and one double loop event changed in a complex and undetermined manner, with reconnection being one possibility.

5. The rise time, decay time and rate of increase of soft x-ray emission tended to increase with flare volume.
6. There were no correlations evident between either the maximum soft x-ray emission or the observation of non-thermal radio bursts with other flare observables.
7. The eight flares which underwent a large scale deformation tended to be thicker and have larger volumes, longer rise and decay times and smaller time rates of change of their soft x-ray emission in both the rise and decay phases.

Based on observation of flare evolution in the original film, it is suggested that the eight flares which underwent a large scale deformation have become kink unstable.

6. DISCUSSION

The most significant results obtained from the present study of limb flares are the observations of large scale deformations of flare loops that occurred during the course of several events and the small scale short-lived perturbation to a flare loop that was observed immediately before a type III burst. In this section some possible physical implications of these results are discussed.

For this discussion it will be assumed that the large scale deformations were the result of MHD kink instabilities. This assumption is motivated by the resemblance in the original film of the evolution of the deformation to a kink. In cylindrical coordinates the kink deformation of an axial flux tube is defined by $m = \pm 1$ where m defines the azimuthal mode of the perturbation, which varies as $\exp i(kz + m\theta)$. For either $m = +1$ or -1 the perturbation is a helix or screw, while the sum of the two perturbations having $m = +1$ and -1 define a buckling which takes place in one plane only. Observations of disc flares in the initial study did not reveal any large scale helical geometry which therefore favors deformation in one plane only.

The presence of an MHD kink instability in a magnetic flux loop is caused by the flow of an axial component of current which becomes large enough to make the induced azimuthal magnetic field, B_θ , approximately the same magnitude as the axial field, B_z . Let us consider a cylindrically symmetric magnetic flux tube which has negligible pressure gradients and determine under what conditions the total magnetic stress in the direction along the tube axis will go from tension to compression. This is an approximate

measure of when it becomes unstable to buckling. The Maxwell stress on the $z = \text{constant}$ surface in the z direction is (Jackson, 1962)

$$T_{zz} = \frac{1}{2\mu_0} (B_z^2 - B_\theta^2) \quad (3)$$

For a tube of radius a , the total magnetic stress in the z direction is

$$T_z = \frac{\pi}{\mu_0} \int_0^a (B_z^2 - B_\theta^2) r dr \quad (4)$$

From Ampere's law,

$$B_\theta = \frac{\mu_0}{r} \int_0^r J_z(r') r' dr' \quad (5)$$

Thus, from (4) and (5) it is concluded that for a given B_z distribution, a flux tube tends to become unstable to bucking ($T_z = 0$) as either the level of the total axial current is increased or as the distribution of current becomes more concentrated towards the tube's axis. This same general conclusion should also be valid for a curved flux tube where the radius of curvature is much larger than the radius of the tube.

Since only eight out of 15 limb flares were observed to undergo a large scale deformation, the kink instability cannot be regarded as the primary flare mechanism. Rather, it is useful to explore the possibility that the strong currents flowing along the flux tube are always a major causal element in the flare process and that kinking occurs only when the current level and distribution create the proper conditions. This is consistent with the observations that "kink" flares tend to have longer rise and decay times and smaller rates of increase and decrease of soft x-ray emission. That is, in "kink" flares,

some of the energy which would otherwise go into electromagnetic radiation is converted into kinetic energy of the moving flux tube. In the decay phase, some of this energy is given back to the radiation field as the moving particles thermalize. For an estimate of this kinetic energy, assume a volume of $3 \times 10^{26} \text{ cm}^3$, a density of 10^{11} cm^{-3} and a displacement of 20 arc seconds in one minute of time (a velocity of 240 km/sec). These values yield an energy of 1.5×10^{28} ergs which is approximately one order of magnitude less than the energy released in small flares (Kane, 1973). It is also seen that this energy corresponds to a small decrease in the free magnetic energy of a twisted flux tube. That is, for the above volume and energy change, the corresponding decrease in a 100 gauss azimuthal field is only 6 gauss.

The link between strong currents and flares may be evident in another way. Flare knots of emission seen in $H\alpha$ are located adjacent to magnetic neutral lines and 80% of the time they coincide with the sites of the strongest electric currents flowing through the photosphere (positive or negative) determined by observation of the transverse magnetic fields and Ampere's law, $\vec{J} = \nabla \times \vec{H}$ (Moreton and Severny, 1968). If the assumption is made that the $H\alpha$ flare knots are the footpoints of the loops observed in soft x-rays, then it is concluded that flares occur in flux tubes through which significant current is already flowing.

It is also evident in a third way that the regions of large current are favorable for the occurrence of flares. Flares tend to occur where magnetic field gradients are high, which from Ampere's law usually requires high currents. These currents are considered to be flowing in the photosphere and

below, but could also easily flow along flux tubes extending higher into the atmosphere. In the corona, where the gas pressure is small with respect to the magnetic field pressure, the net current flow is essentially restricted to follow magnetic field lines. In the photosphere and below, this restriction does not hold and currents can be induced to flow in any direction as the frozen-in magnetic fields are pushed about by the atmospheric dynamics. In particular, twisted flux tubes extending out of the photosphere requires a current flow along them. Related to this is the observation that the amount of twist evident in an active region can be related to the amount of flare energy stored and released (Tanaka and Nakagawa, 1973). It should also be noted that we need not always restrict our attention to one flux tube only. We observe more than one flux tube in 3 out of 26 flares. Also, it has been observed that a flare may consist of a successive release of energy from several flux tubes forming an arcade (Vorpahl, 1976).

As yet, there are no direct observations available on the exact nature of the current flow during a flare. Ideally, one would like to have high spatial and time resolution observations of the total magnetic field (longitudinal and transverse) at the site of a flare. Slightly less difficult, but very useful, would be high spatial and time resolution observations of the line-of-sight field at the location of limb flares. At present, we do not know how the current through a tube is distributed with distance away from its axis, how this distribution changes with time or even how the total current changes with time.

It is natural to expect that the total current through a flux tube could not change significantly during a flare because of the large inductance of the circuit involved. However, since the coronal plasma is highly conducting, the plasma adjacent to the flux tube effectively screens the main body of the corona from flux changes that are caused by a change in the total current. In this way, the self inductance of a flux tube can be substantially reduced. The screening is accomplished by the flow of surface current over the tube which is approximately equal in magnitude and opposite in direction to the net change of current inside the tube. If there is appreciable Joule heating associated with this surface current, it could be the reason the flux tubes appear so sharply defined during the flare rise phase. If some of the flux change is not contained by the surface currents, kinetic energy is added to the surrounding solar plasma. That is, over distances large compared to a skin depth, the field and plasma are frozen together

$$\vec{v} \cdot \nabla \vec{B} = - \frac{\partial B}{\partial t} \quad (6)$$

and the plasma is accelerated to compensate for the changing field. Thus, the possibility of a current surge or surges causing both the flare itself and the kink instability cannot be ruled out until the details of the screening are analyzed.

It is useful to discuss these limb flare observations with respect to some of the existing concepts of the flare mechanism. It might initially be thought that the faint spike sometimes observed at the top of a flare loop would tend to support the current sheet tearing mode instability model (Carmichael, 1964; Sturrock and Coppi, 1966; Barnes and Sturrock, 1972). However, since almost all of the soft x-ray emission comes from the

loop itself, these observations offer no evidence for an energy release along the spike, which might be identified with the neutral sheet. This, in no way, disproves the model, however, since the emission measure of a current sheet could be considerably smaller than that of a loop. An alternate explanation of the spike is found in the short-lived small scale perturbation of a loop that was observed immediately preceeding a type III radio burst (Figure 4). Energetic events of this kind could blow out some of the weaker magnetic field at the upper edge of a flux tube to form open field lines. Material or energy, or both, would then have an easy path to travel upward and form the observed spike. Also relevant to this current sheet tearing mode model, is the fact that it does not explain the observed large scale deformations to the flare loops. This model, although presently receiving much attention and excellent analysis, was motivated by the theoretical question on how a highly sheared magnetic field in the corona can rapidly reconnect and thereby release energy (Petschek, 1963). This mechanism of magnetic field annihilation is certainly applicable to many phenomena on the sun, including flares, but the location and geometry of the energy release in the model is not supported by the observations reported here.

The current interruption model (Alfvén and Carlqvist, 1967; Carlqvist, 1969) focuses attention on the role of current flow in flux tubes. It predicts that an instability in the current flow causes a rapid conversion of stored magnetic energy (high inductance) into thermal, kinetic and electromagnetic forms and thereby produces a flare. However, like the previous model, it also does not explain the observed large scale deformation of a flare loop.

The release of flare energy is also attributed to the upward propagation of Alfvén twist waves along flux tubes (Piddington, 1973 and 1974). The tubes are assumed to be twisted before emerging and their subsequent unwinding releases the flare energy. This model, although it does not explicitly account for the observed large scale deformation, does attribute flares to twisted flux tubes and in this sense is consistent with the flow of large currents that have been inferred from the present observations. However, we do not require that the twist exist before the flux tube emerges. The twist may build up slowly before a flare, or rapidly, as in a current surge.

One other model which is consistent with our observations, as well as our interpretation of them, predicts a preflare current enhancement in a loop because of superheating and current convective instabilities (Spicer, 1975). In essence, the superheating instability depends upon the fact that the Coulomb cross section for momentum transfer for electrons decreases as v^{-4} , where v is the relative velocity of an electron and the other charged scattering particle. Assuming a Boltzmann velocity distribution, the electrical conductivity varies as $T^{3/2}$. Superheating occurs when the Joule heating exceeds the radiative power loss and the temperature, conductivity and Joule heating therefore increase in a runaway fashion. This continues until a sufficiently large power loss mechanism brings it to a halt, most likely the instability which is responsible for the release of most of the flare energy. At the same time that this superheating is occurring, and really as part of the same process, the current convective instability causes current to concentrate in regions where the conductivity was initially high. It is in these regions that superheating has its

greatest effect. If these regions of the flare loop are on its axis and the total current becomes high enough, the resulting axial concentration of current would make the loop kink unstable. In any case, the high gradients in current density resulting from the current concentration could be responsible for a subsequent tearing mode instability which releases much of the flare energy. The details of this model are yet to be analyzed.

Before leaving the subject of flares and large scale MHD instabilities, it should be noted that there may be similarities between the large scale flare loop deformation and the eruption of very large twisted prominences. Unlike flare loops, the prominences are large enough that a definite twist or fine scale helical geometry can be seen in them as they erupt. For example, this is evident in the 4 June 1946 eruption, the largest ever photographed (displayed in Gibson, 1973 or Zirin, 1966) and the more recent one recorded from Skylab at 0635 UT on 19 December 1973 (displayed in Gibson, 1974).

One other flare observation which merits separate discussion is that of the small short-lived deformation observed in a segment of a flaring loop 10 seconds before the beginning of a type III burst (Figure 4). The obvious question is how this deformation was related to the burst of non-thermal electrons which moved outward through the corona and excited plasma waves. One possibility is that a concentrated release of energy occurred on the loop in a volume with a characteristic size of 1 arc second or less. Material was subsequently ejected upward, forming the observed deformation, as high energy electrons were injected into the corona. A second possibility is that part or all of the left side of the loop deformed rapidly into a kink and that the electron

burst was a result of this MHD instability driven deformation. This latter possibility is now briefly explored.

A possible source of acceleration for the electrons was the $\vec{v} \times \vec{B}$ electric field induced by the rapid deformation. The velocity corresponding to the observed change was at least 100 km/second. The magnetic field, into which the deformation moved, was equal to the initial ambient field minus the field due to currents convected with the deformation. Its magnitude is here assumed to be 1 gauss so that an induced electric field of 10^4 volts/km results. Thus, for electrons to be accelerated to one third the speed of light would have required a distance of only 2-8 km, which is small with respect to the electron mean free path. That is, assuming a coronal density of 10^9 protons/cm³ and a Coulomb multiple scattering cross section for a thermal electron (0.1 keV) of 3×10^{-16} cm² (Krall and Trivelpiece, 1973), an electron mean free path of 33 km is calculated. As an electron is accelerated, its mean free path increases as v^{-4} and it would therefore have always been much larger than the acceleration distance.

Regardless of the source of electron acceleration, the mechanism must be capable of producing the observed nominal total energy and electron fluxes which are 3×10^{28} ergs and 7×10^{35} electrons, respectively (Kane, 1973). It was seen earlier that a decrease of only 6 gauss in a 100 gauss azimuthal field over a volume of 3×10^{26} cm³ releases 1.5×10^{28} ergs. Thus, the partial untwisting of a segment of a flux tube could account for the energy of the non-thermal electrons. However, the number of electrons emitted by a typical type III radio burst is a more difficult matter. The emitted electron flux is essentially a current flow which creates a very strong, if only transient

magnetic field which is given approximately by

$$B = \mu_0 I/L \quad (7)$$

$$= \mu_0 e N/L \Delta t \quad (8)$$

where I is the current, L is the characteristic circumference of the current flow, N is the total number of emitted electrons and Δt is the time of emission. Assuming conservative values of 10^4 km, 10^{35} electrons and 10 seconds for these parameters, a field of 2×10^6 gauss results. It must be concluded that mechanisms which could induce a large scale field of this magnitude and dynamically balance the resulting high magnetic pressure are presently unknown.

ACKNOWLEDGEMENTS

Gratitude is expressed to the entire NASA Skylab team which made the acquisition of this data possible and to Mr. James E. Milligan who served as S-056 Principal Investigator for much of the duration of this experiment. The High Altitude Observatory's S-052 experiment team, led by Dr. Robert MacQueen, is thanked for allowing the author to review their coronagraph data covering the time periods surrounding the flares investigated here. The author wishes to acknowledge most constructive discussions with Drs. Chung C. Cheng and Daniel Spicer of the Naval Research Laboratory on the theory of flares in magnetic flux tubes. Useful critical comments on the paper were received from Drs. George Paulikas, Hugo Rugge, James Underwood, Joan Vorpahl, David McKenzie and Peter Landecker of The Aerospace Corporation. Appreciation is also given to Robert J. Maulfair and Georg E. Schacht for their knowledgeable and patient work in the darkroom. This work was performed under NASA Contract NAS8-29602.

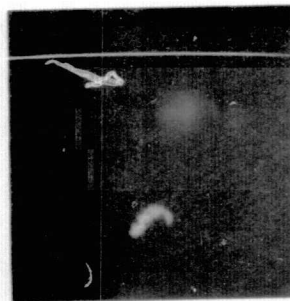
FIGURES

1. Limb Flare Loop. This C2 flare occurred at S15W71 ($R/R_{\odot} = 0.95$) and is shown here approximately 1/2 minute before the Be(2-8Å) X-REA counter maximum at 0209 UT. The limb location is shown by the white curved line. The 3.75 second exposure was taken using a beryllium filter having a 6-18Å passband.
2. Measurements Made on Limb Flare Loops.
3. Triangular Flare Loop Geometry Near Maximum.
 - a) Triangle Plus Faint Spike. The spike, although very faint in this reproduction, is much more clearly seen in the original film where it appears to be a smooth continuation of the underlying structure. In fact, it resembles a small helmet streamer. This is depicted in the sketch to the right of the photograph. This C5 flare occurred at S13W90 ($R/R_{\odot} = 1.00$) and reached a maximum in the 2-8Å counter at 1215 UT. Another photo of this flare taken through a different filter is shown in Figure 9 of the Initial Study.
 - b) Growth of a Loop Into a Triangular Structure. It is possible that this change was due to a kink instability that had not progressed as far as in the sequence shown in Figure 5 or it may correspond to stages I and IV, shown there. This C1 flare occurred at S18E65 ($R/R_{\odot} = 0.92$) and reached a maximum in the 2-8Å counter at 1356 UT.
4. Small Scale Flare Loop Perturbation Immediately Preceding a Type III Radio Burst. The perturbation is indicated by the arrow in the 1425:02 UT frame. This C6 flare occurred at N7W84 ($R/R_{\odot} = 0.99$) and reached a maximum in the SOLRAD 1-8Å channel at 1428 UT.

5. Large Scale Deformation of a Flare Loop. The data shown in a) is interpreted in b) where a kink instability of the original loop is depicted. This C5 flare (inferred from X-REA data) occurred approximately 10° over the west limb at a latitude of 7° north. It reached a maximum at 2200 UT.
6. Measured 2-8Å Soft X-ray Flux for the Flare shown in Figure 5.
7. A Two Loop Flare. This M1 flare occurred at S13W64 ($R/R_\odot = 0.91$) and reached a maximum in the 2-8Å counter at 1517:30 UT.
8. Measured 2-8Å Soft X-ray Flux for the Flare shown in Figure 7.
9. Flare Loop Geometry Correlations. The correlation coefficients are: a) +0.132 and b) +0.304.
10. Rise Time, Decay Time and Flare Volume Correlations. The correlation coefficients are: a) +0.709, b) +0.714 and c) +0.512.
11. SOLRAD Peak Flare Intensity Correlation with Flare Volume. The correlation coefficient is -0.317.
12. Correlations of the Characteristic Rates of Rise and Decay of Soft X-Ray Emission with Flare Volume. The correlation coefficients are: a) -0.762 and b) -.0434.
13. Correlations of Evidence for Kink Evolution with Other Flare Observables. The correlation coefficients are: a) +0.633, b) +0.554, c) +0.578, d) +0.737, e) -0.456, f) -0.847 and g) -0.598.
14. Sample Correlation Coefficients and 95% Limits of Confidence for All Correlations Studied. See text for details.

3 DEC 73

0208 : 29 UT



10 arc sec

3.75 sec
Be(6-18Å)

Fig.
1

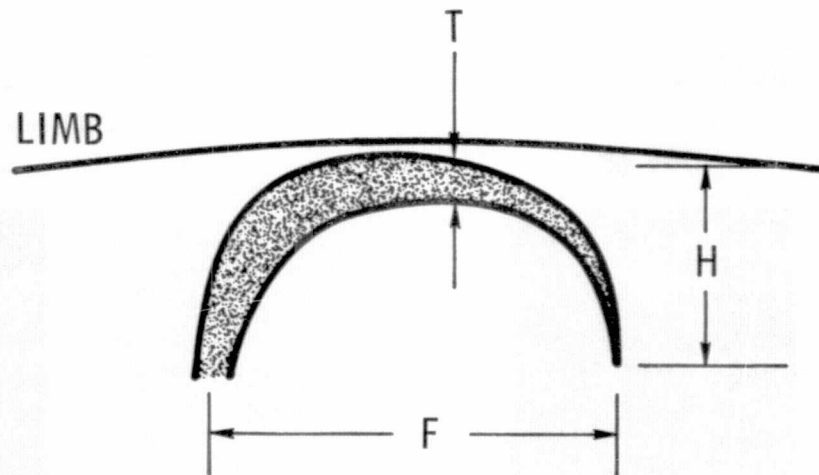
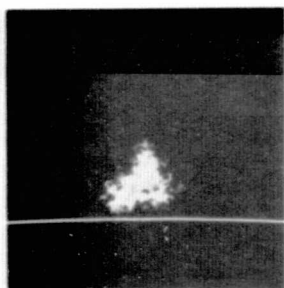


Fig.
2

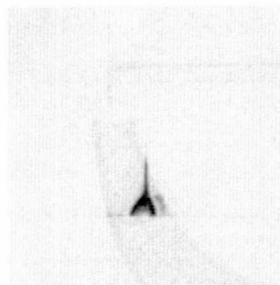
a) 6 SEP 73

1220 : 11 UT



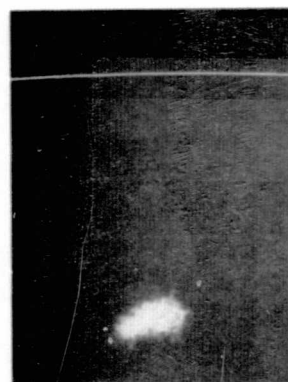
53 sec

Be (6 - 13Å)



b) 1 SEP 73

1356 : 14 UT



49 sec

Ti (6-14, 27-47 Å)

1402 : 22 UT

10 arc sec

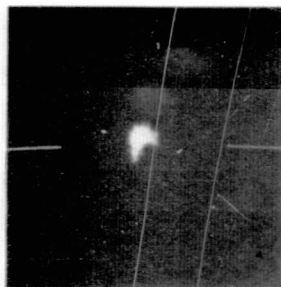


14.5 sec

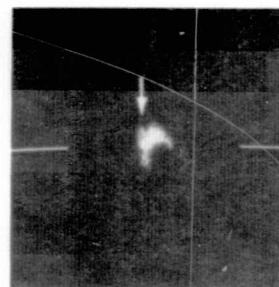
Fig.
3

15 JAN 74

1424 : 34 UT



1425 : 02 UT

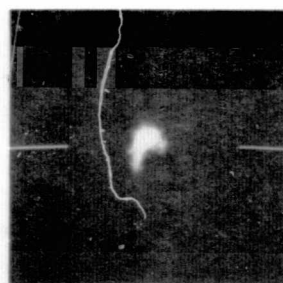


10 arc sec

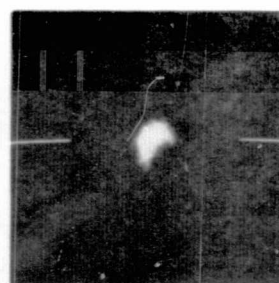
1425 : 29 UT



1425 : 57 UT



1428 : 41 UT



1.25 sec, Be(6-13 Å)

Fig.
4

16 JAN 74

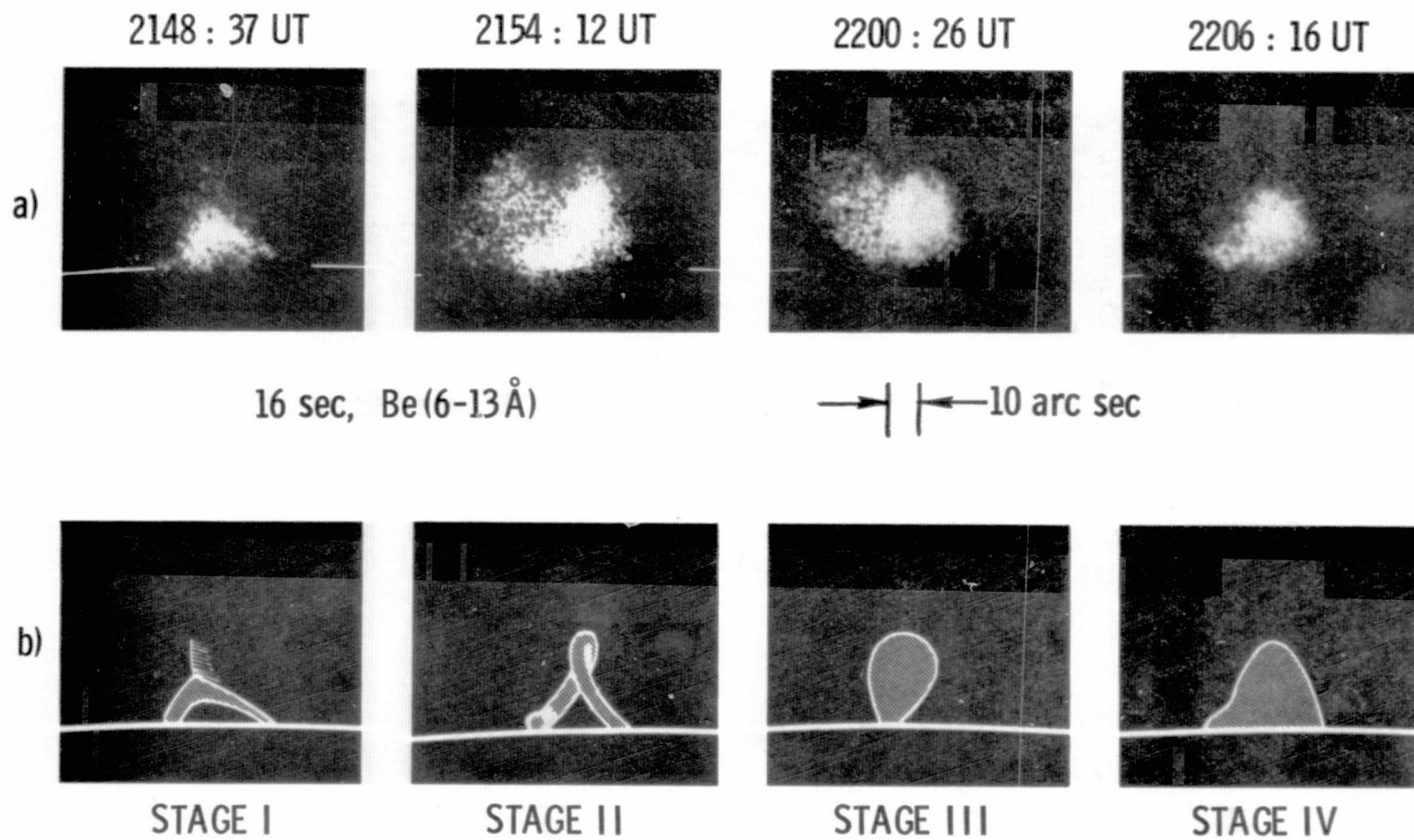


Fig.
5

16 JAN 74

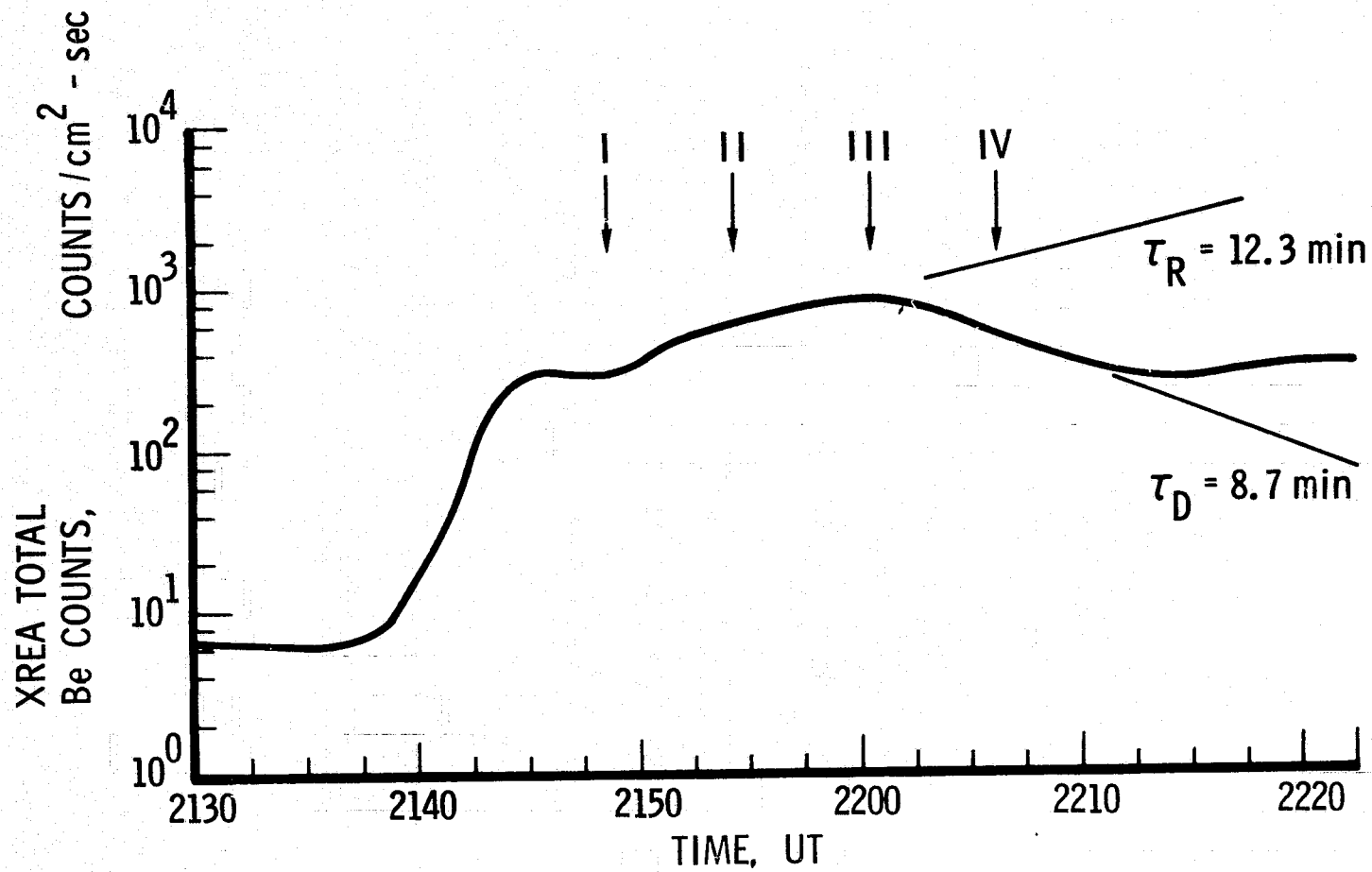


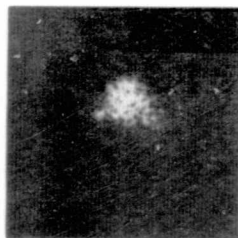
Fig.
6

2 DEC 73

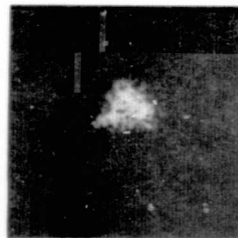
1515 : 57 UT



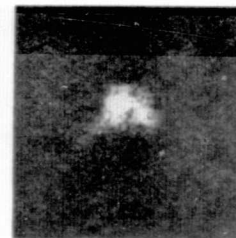
1516 : 24 UT



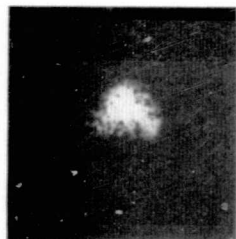
1516 : 52 UT



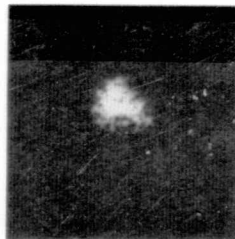
1517 : 19 UT



1517 : 46 UT



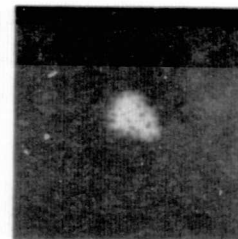
1518 : 41 UT



1518 : 14 UT



1519 : 09 UT



1.25 sec, Be(6-13Å)

→ | ← 10 arc sec

Fig.
7

2 DEC 73

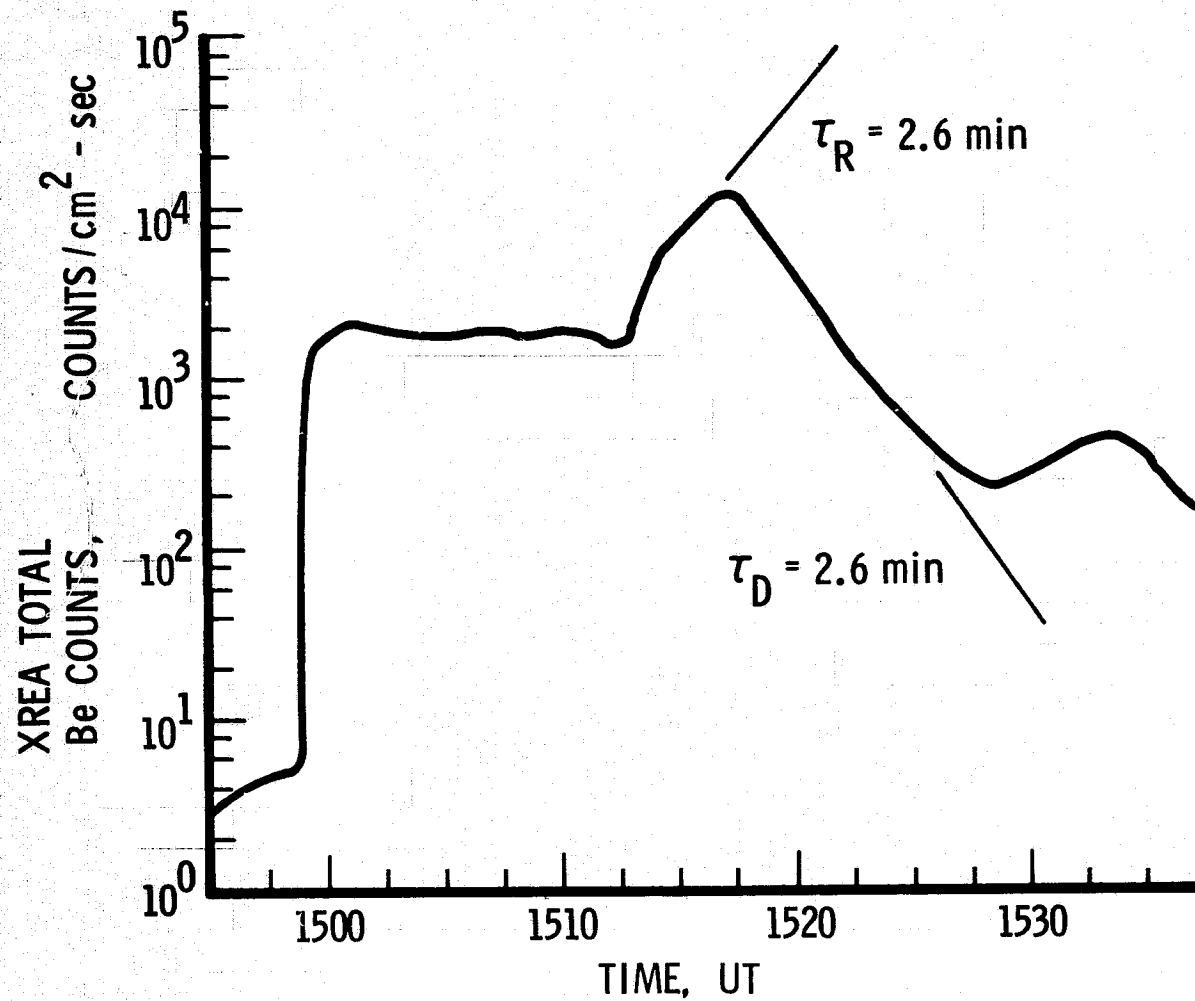


Fig.
8

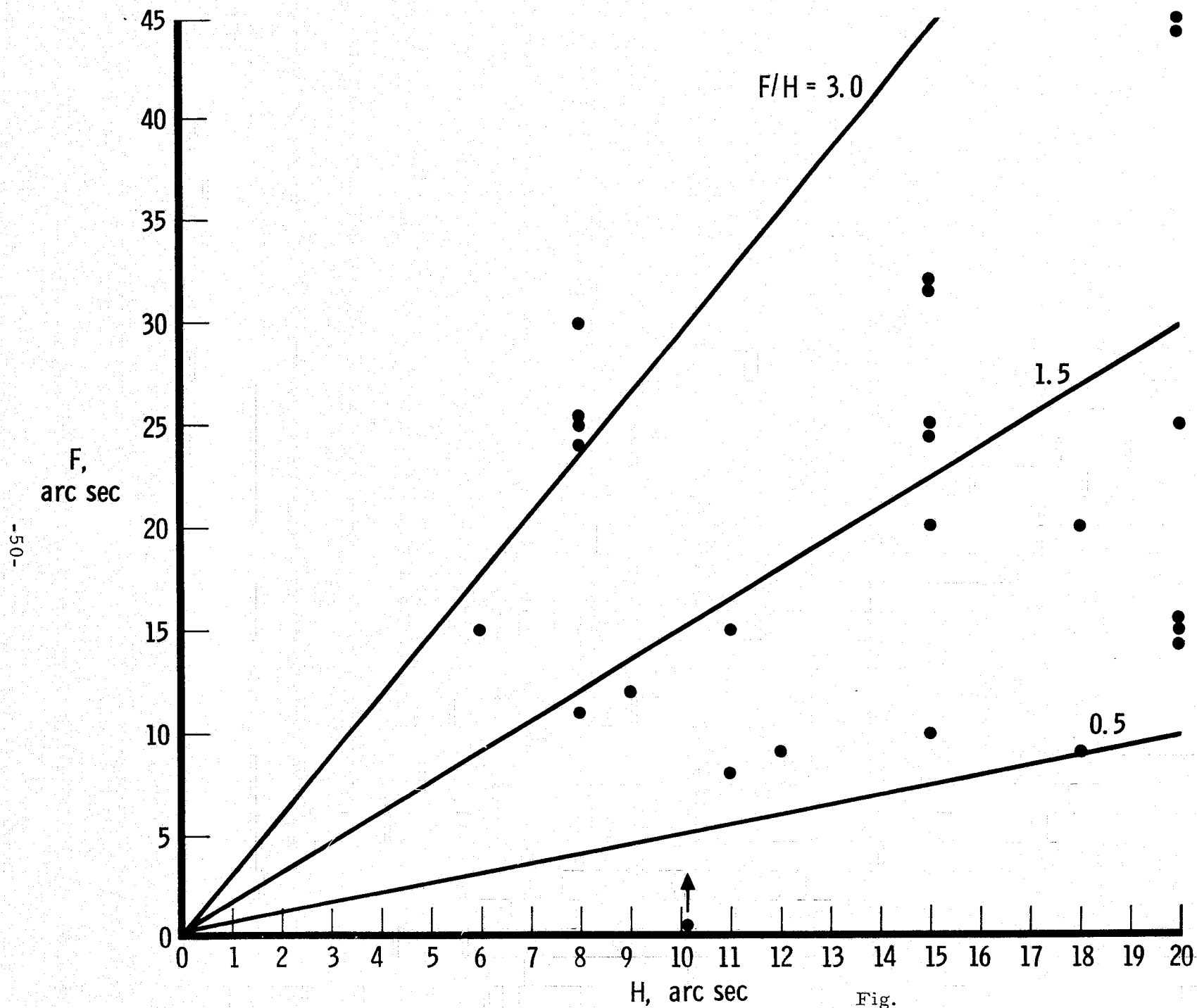


Fig.
9a

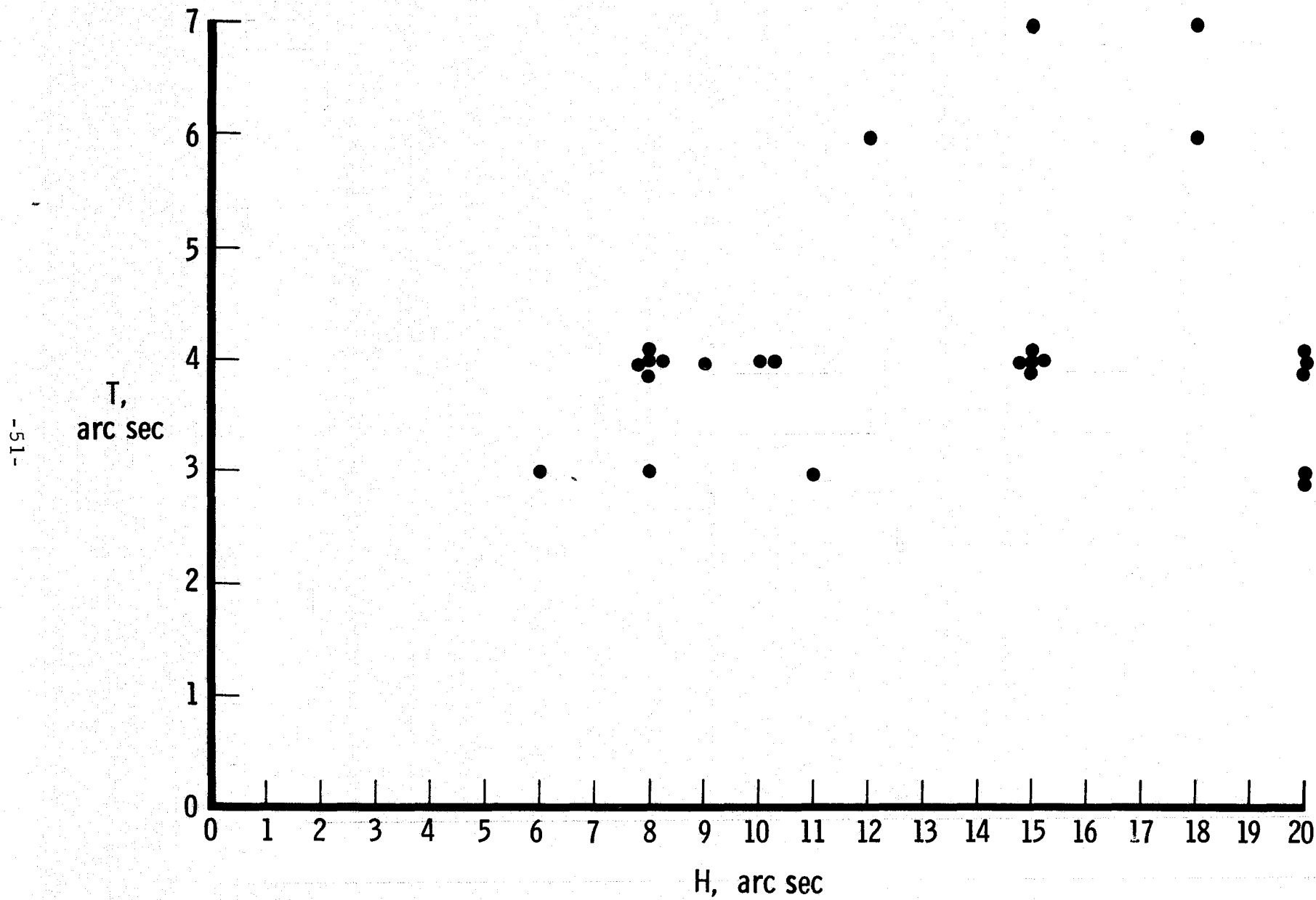


Fig.
9b

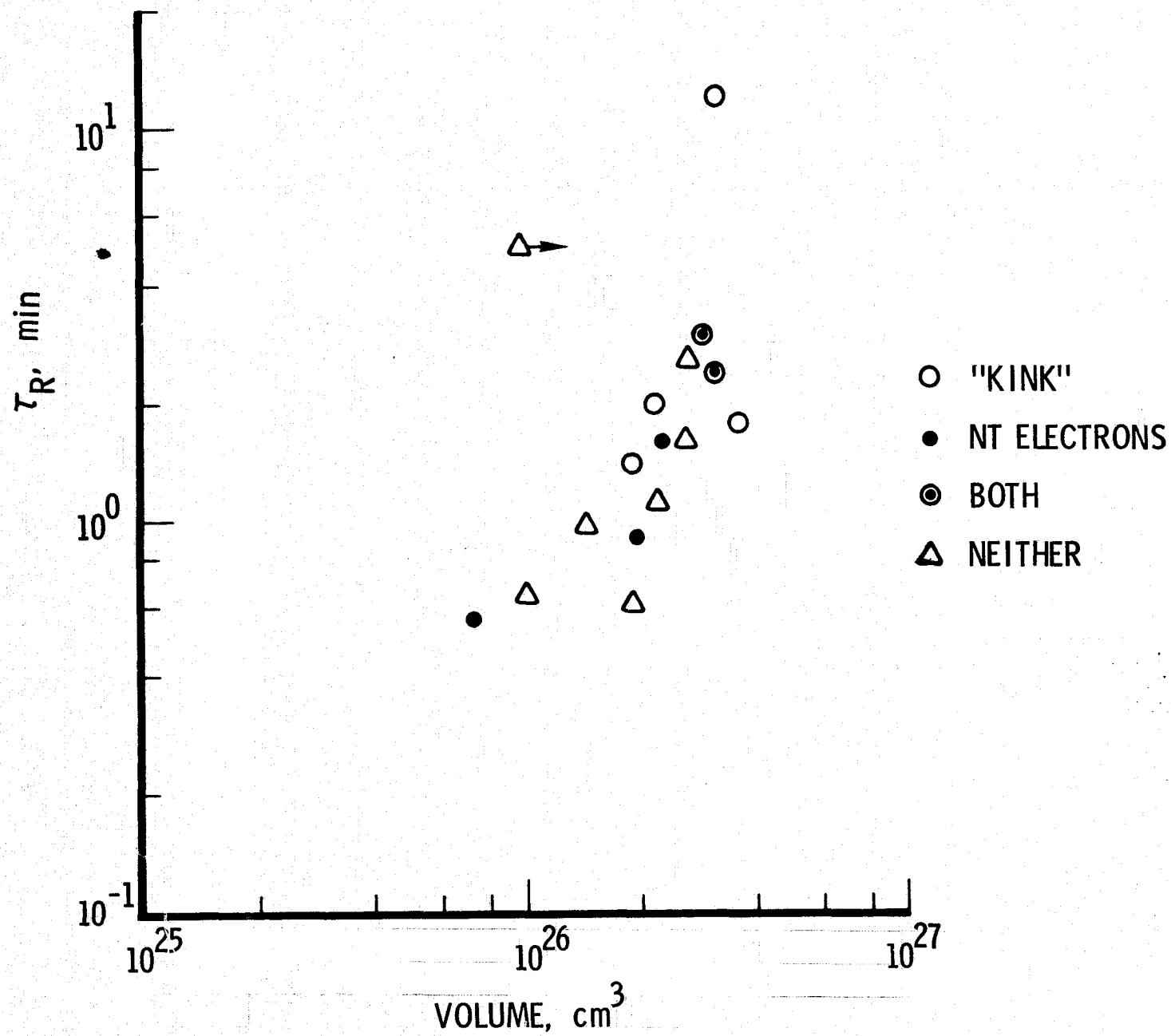


Fig.
10a

Fig.
10b

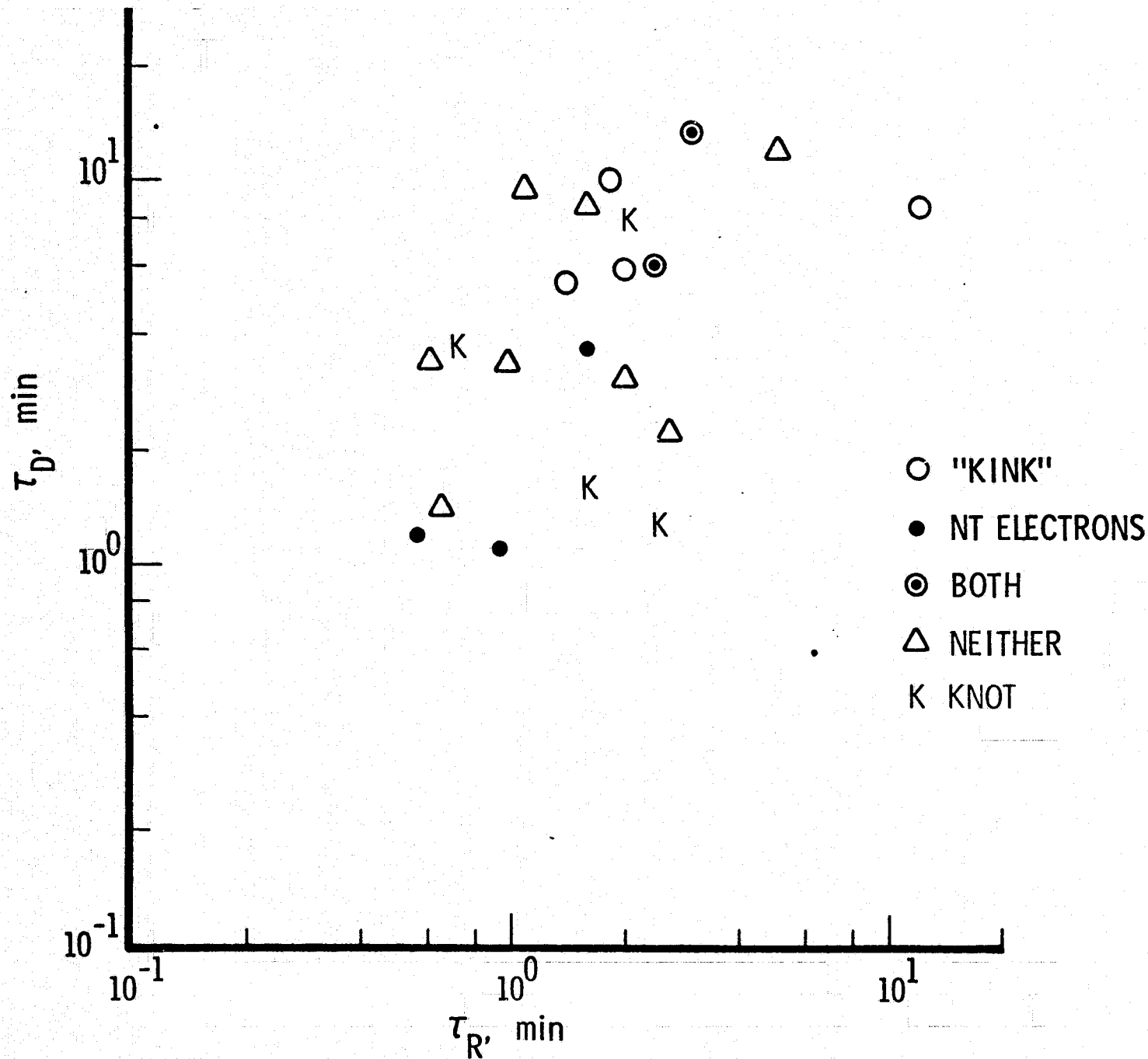


Fig.
10c

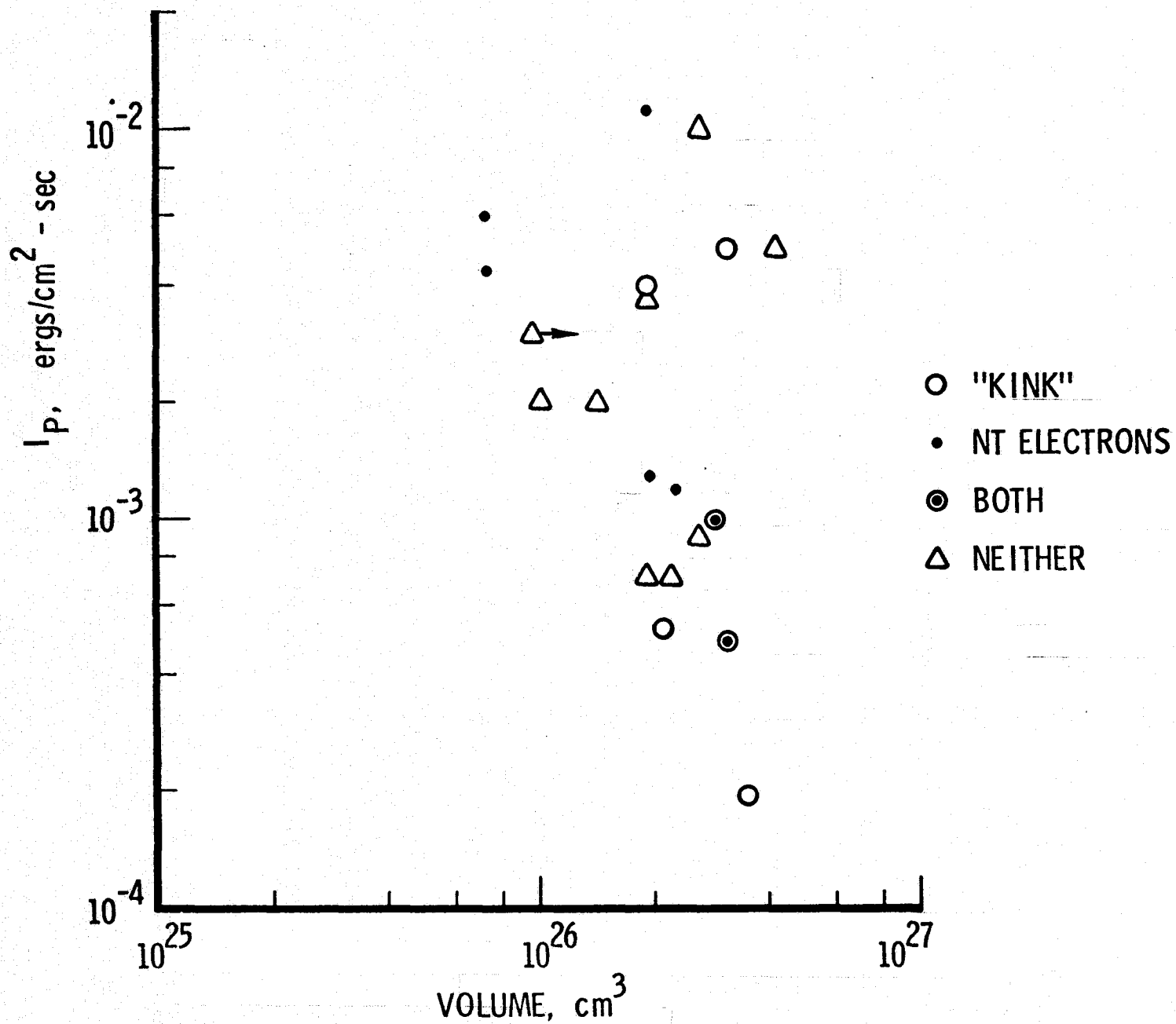


Fig.
11

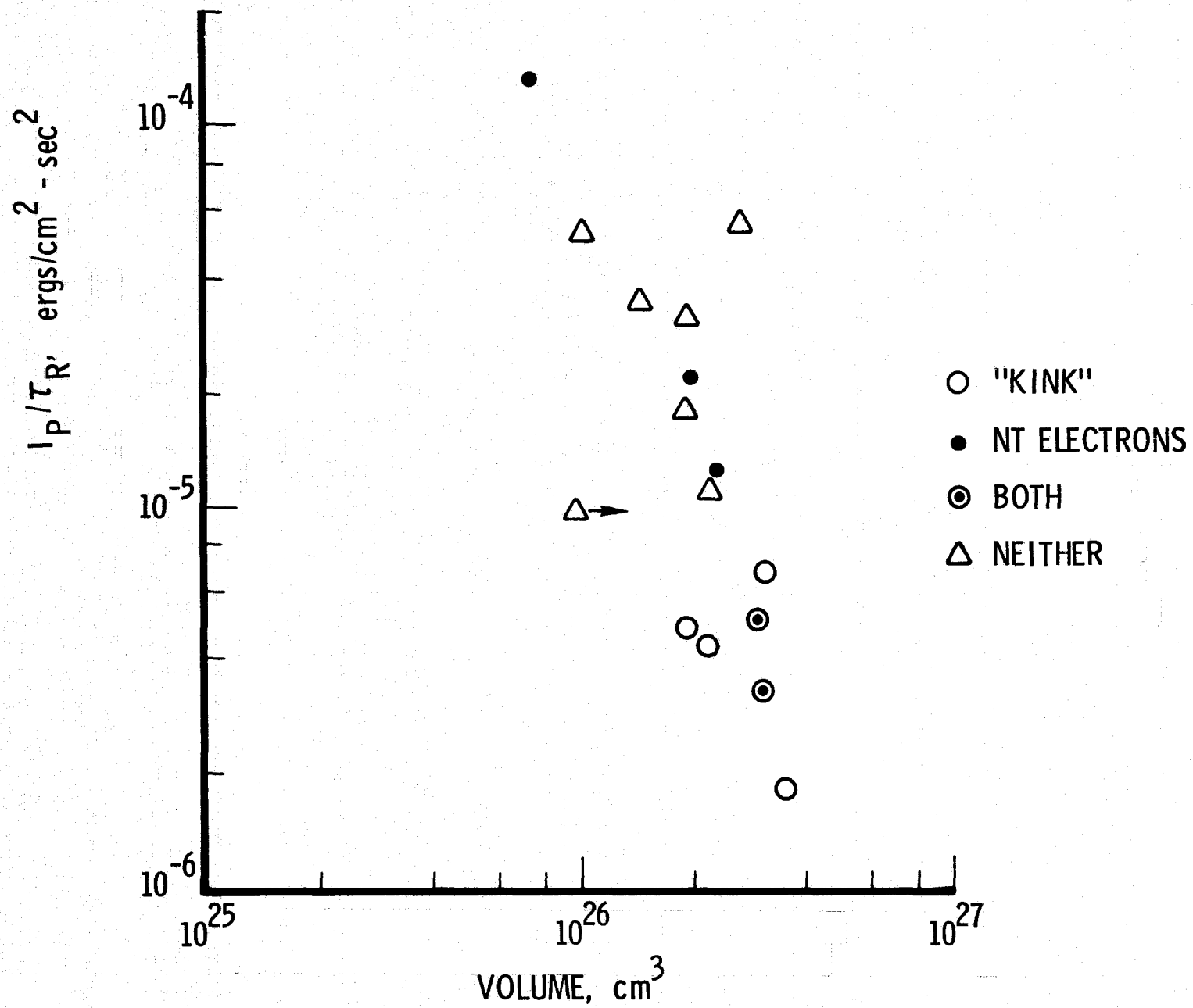


Fig.
12a

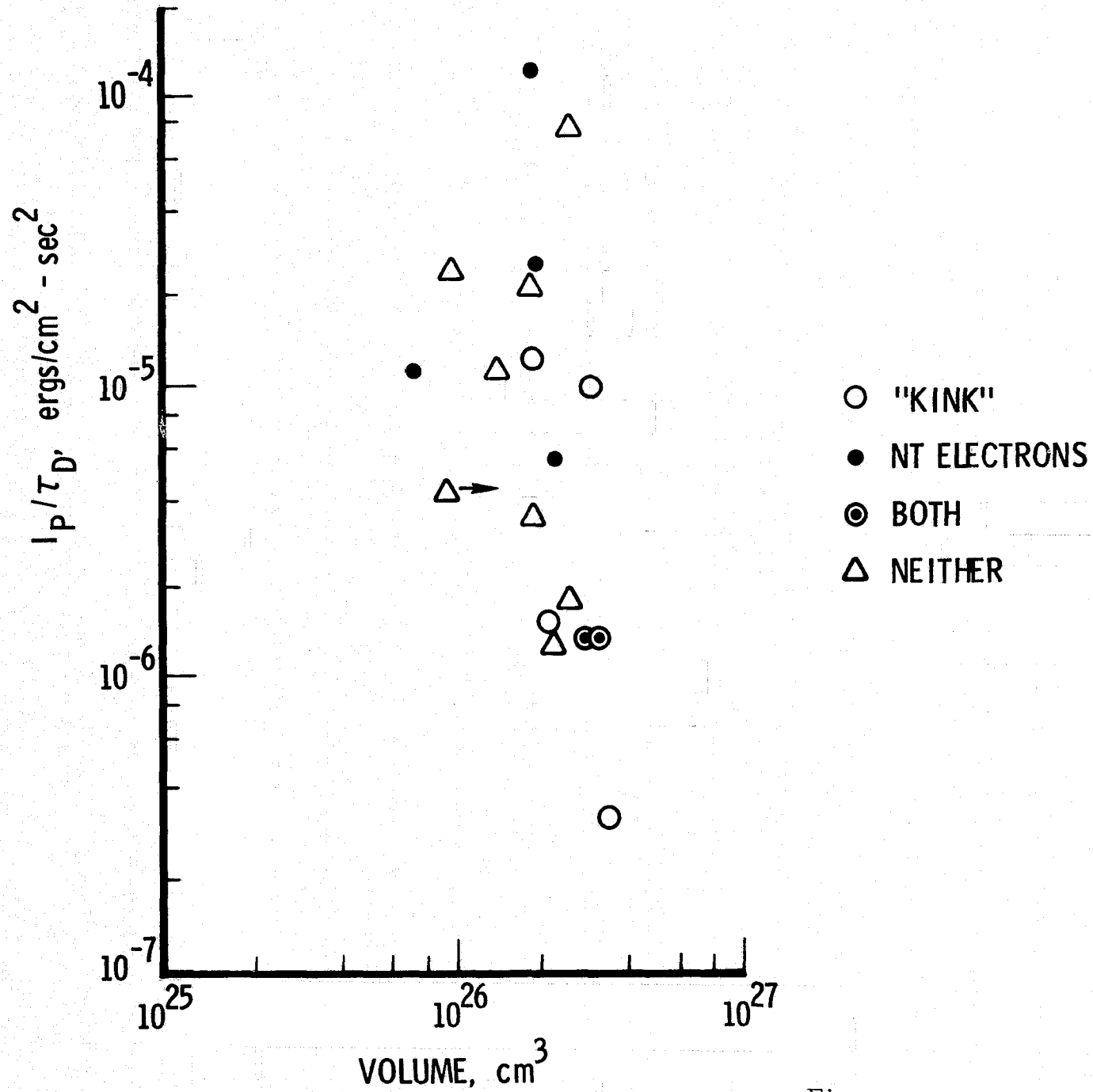
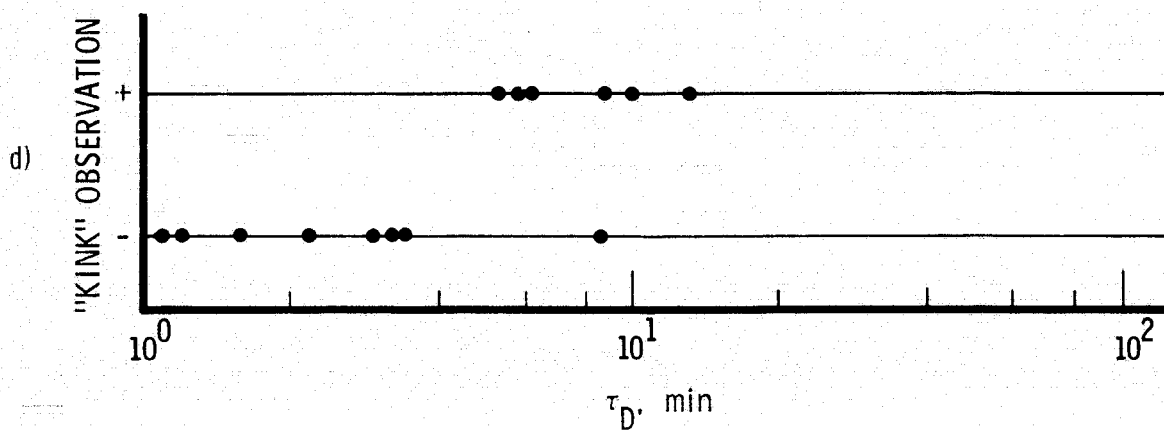
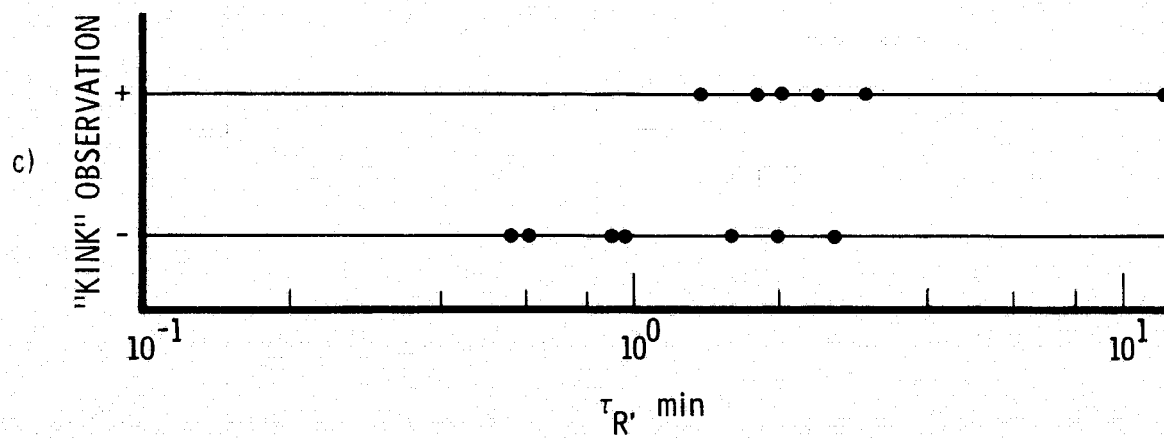
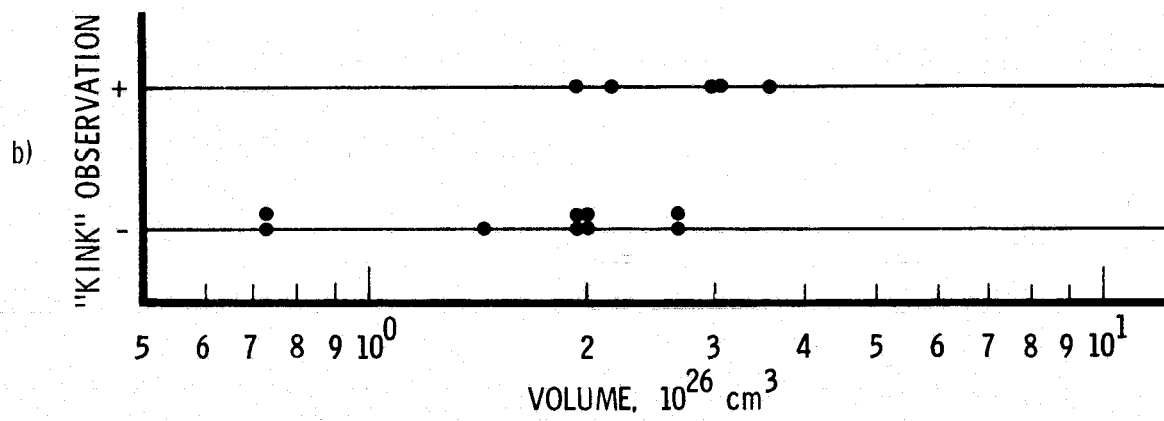
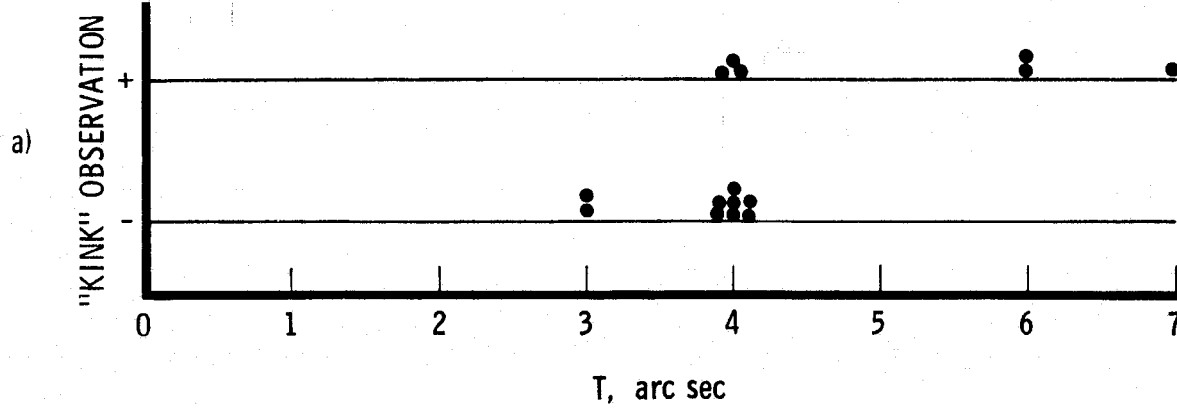
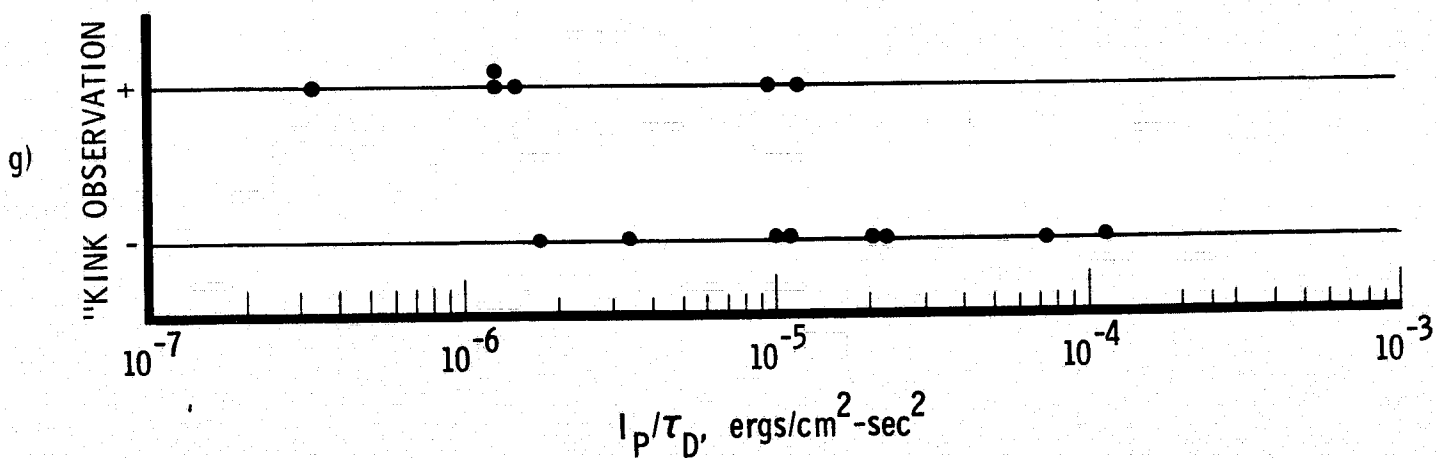
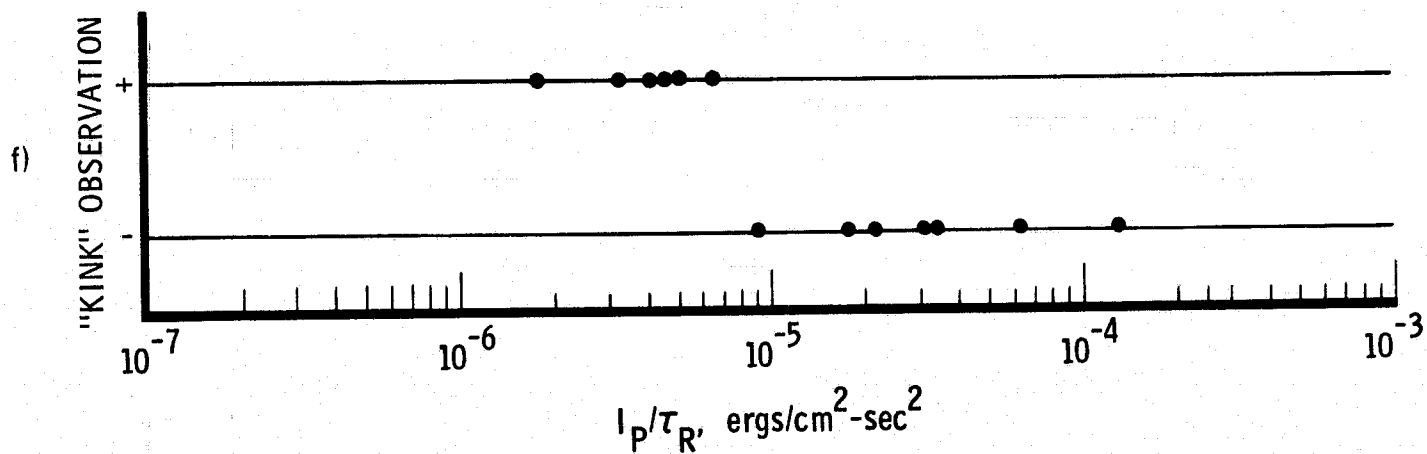
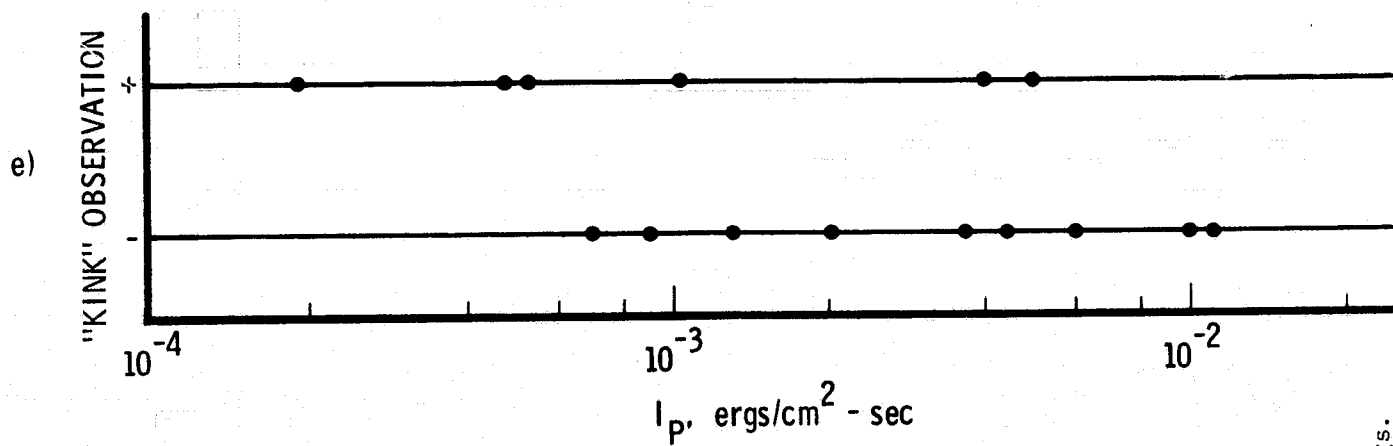


Fig.
12b



Figs.
13a-
13d



Figs.
138 -
139

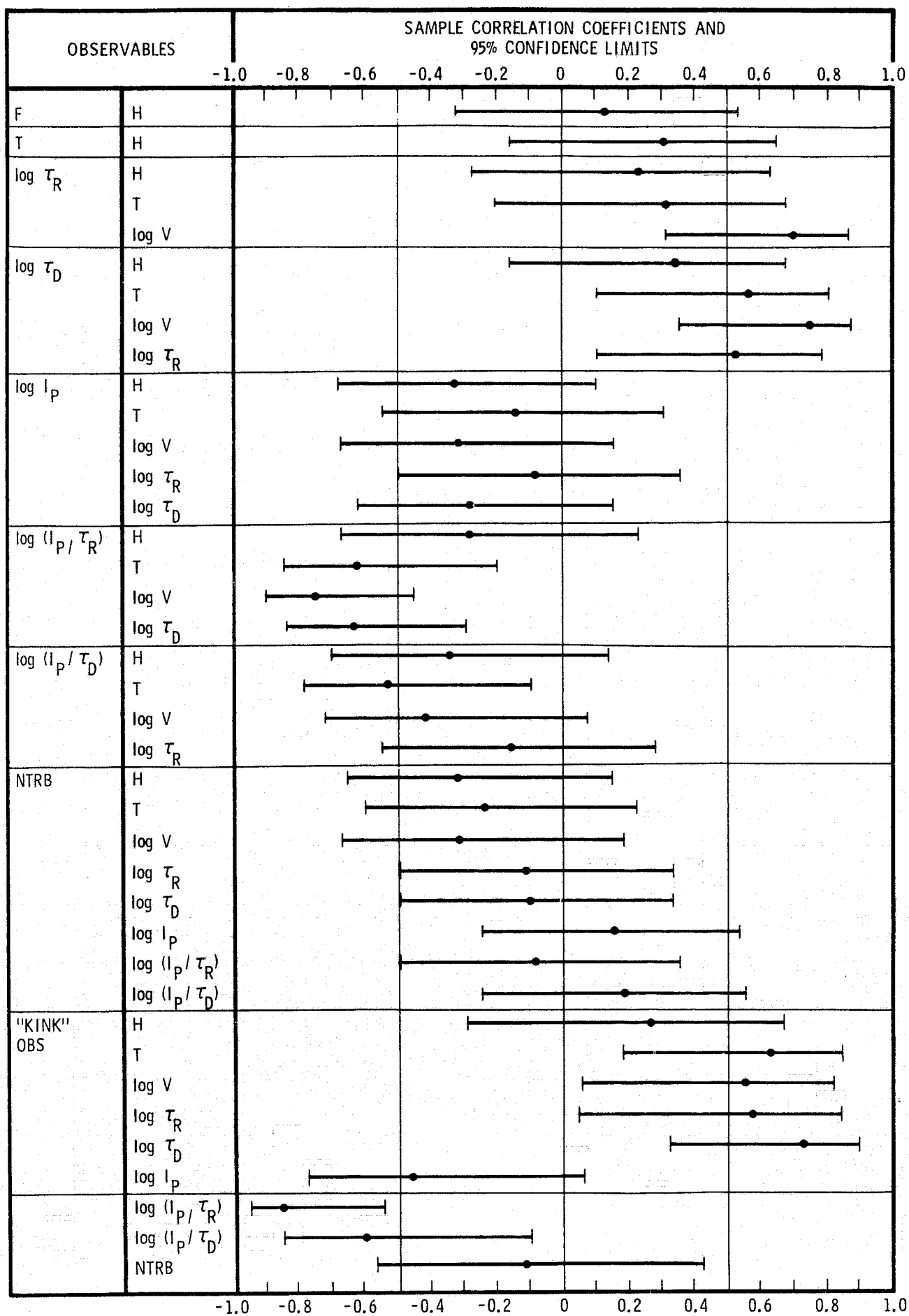


Fig.
14

REFERENCES

- Alfven, H. and Carlqvist, P.: 1967, Solar Phys. 1, 220.
- Barnes, C. W. and Sturrock, P.A.: 1972, Astrophys. J., 174, 659.
- Beyer, W.H.: 1966, Handbook of Tables for Probability and Statistics.
Cleveland, Ohio: The Chemical Rubber Co. (pages 154-159).
- Carlqvist, P.: 1969, Solar Phys. 7, 377.
- Carmichael, H.: 1964, in W.N. Hess (ed.), The Physics of Solar Flares.
NASA SP-50, p. 451.
- Cheng, C.C.: 1975, private communication.
- Cheng, C.C. and Widing, K.G.: 1975, Ap. J. in press.
- Gibson, E.G.: 1973, "The Quiet Sun", NASA SP 303, p. 66.
- Gibson, E.G.: 1974, "The Sun As Never Seen Before", Journal of the
National Geographic Society, 146, No. 4 (October), p. 502; Photo
supplied by R. Tousey, J.D. Bohlin and J.D. Purcell of NRL.
- Jackson, J.D.: 1962, "Classical Electrodynamics", J. Wiley & Sons,
New York, p. 194.
- Kane, S.R.: 1973, in R. Ramaty and R.G. Stone (ed.), High Energy
Phenomena on The Sun, NASA SP 342, p. 55.
- Krall, N.A. and Trivelpiece, A.W.: 1973, "Principles of Plasma Physics",
McGraw-Hill, New York, p. 294.
- Moreton, G.E. and Severny, A.B.: 1968, Solar Phys. 3, 282.
- Munro, R.H., Gosling, J.T., Hildner, E., MacQueen, R.M., Poland, A.I.,
and Ross, G.L.: 1974, Observations of Flare Associated Coronal
Dynamics Above $2 R_{\odot}$. Proceedings of Flare Related Magnetic Field
Dynamics Conference, Boulder, Colorado, September 23-25, 1974,
NCAR Technical Note (to be published in Solar Physics).
- Petscheck, A.E.: 1964, in W.N. Hess (ed.), The Physics of Solar Flares,
NASA SP-50, p. 425.
- Piddington, J.H.: 1973, Solar Phys. 31, 229.
- Piddington, J.H.: 1974, Solar Phys. 38, 465.

- Spicer, D.S.: 1975, A Resistive Screw Instability Model of a Solar Flare, presented at AAS 146th Meeting in San Diego, Calif., August 1975.
- Sturrock, P.A.: 1972, Solar Phys. 23, 438.
- Sturrock, P.A. and Coppi, B.: 1965, Astrophys. J. 143, 3.
- Tanaka, K. and Nakagawa, Y.: 1973, Solar Phys. 33, 187.
- Underwood, J.H., Milligan, J.E., deLoach A. C. and Hoover, R.B.: 1976, Space Sci. Inst., (in press).
- Vorpahl, J.: 1976, Astrophys. J. 15 May 1976.
- Vorpahl, J.A., Gibson, E.G., Landecker, P.B., McKenzie, D.L., and Underwood, J.H.: 1975, Solar Phy. (in press).
- Zirin, H.: The Solar Atmosphere, Waltham, MA: Blaisdell, p. 7.